Chapter 2 The Science of LBNE

The Standard Model of particle physics describes all of the known fundamental particles and the electroweak and strong forces that, in combination with gravity, govern today's Universe. The observation that neutrinos have mass is one demonstration that the Standard Model is incomplete. By exploring physics beyond the Standard Model, LBNE will address fundamental questions about the Universe:

What is the origin of the matter-antimatter asymmetry in the Universe? Immediately after the Big Bang, matter and antimatter were created equally, yet matter now dominates. By studying the properties of neutrino and antineutrino oscillations, LBNE is pursuing the most promising avenue for understanding this asymmetry.

What are the fundamental underlying symmetries of the Universe? Resolution by LBNE of the detailed mixing patterns and ordering of neutrino mass states, and comparisons to the corresponding phenomena in the quark sector, could reveal underlying symmetries that are as yet unknown.

Is there a Grand Unified Theory of the Universe? Experimental evidence hints that the physical forces observed today were unified into one force at the birth of the Universe. Grand Unified Theories (GUTs), which attempt to describe the unification of forces, predict that protons should decay, a process that has never been observed. LBNE will probe proton lifetimes predicted by a wide range of GUT models.

How do supernovae explode? The heavy elements that are the key components of life — such as carbon — were created in the super-hot cores of collapsing stars. LBNE's design will enable it to detect the neutrino burst from core-collapse supernovae. By measuring the time structure and energy spectrum of a neutrino burst, LBNE will be able to elucidate critical information about the dynamics of this special astrophysical phenomenon.

What more can LBNE discover about the Standard Model? The high intensity of the LBNE neutrino beam will provide a unique probe for precision tests of Standard Model processes as well as searches for new physics in unexplored regions.

LBNE has been designed to address a wide range of scientific topics using well-characterized, high-intensity, accelerator-based neutrino beams, a long baseline for neutrino oscillations, and a very large, deep-underground detector with excellent particle identification capabilities over a large

range of energies. While maximizing the reach for a core set of scientific objectives, its design — described in Chapter 3 — accommodates the flexibility to extend the scope of measurements as additional resources become available.

2.1 Scientific Objectives of LBNE

The scientific objectives of LBNE have been categorized into primary, secondary, and additional secondary objectives according to priorities developed and agreed upon by the LBNE community and accepted as part of the CD-0 (Mission Need) approval by the U.S. Department of Energy [1].

Primary objectives of LBNE, in priority order, are the following measurements:

1. precision measurements of the parameters that govern $\nu_\mu \rightarrow \nu_e$ oscillations; this includes precision measurement of the third mixing angle θ_{13}, measurement of the charge-parity (CP) violating phase $\delta_{\rm CP}$, and determination of the neutrino mass ordering (the sign of $\Delta m^2_{31} = m^2_3 - m^2_1$), the so-called *mass hierarchy*

2. precision measurements of the mixing angle θ_{23}, including the determination of the octant in which this angle lies, and the value of the mass difference, $|\Delta m^2_{32}|$, in $\nu_\mu \rightarrow \nu_{e,\mu}$ oscillations

3. search for proton decay, yielding significant improvement in the current limits on the partial lifetime of the proton (τ/BR) in one or more important candidate decay modes, e.g., $p \rightarrow K^+\overline{\nu}$

4. detection and measurement of the neutrino flux from a core-collapse supernova within our galaxy, should one occur during the lifetime of LBNE

In a phased approach to LBNE, the goal of the first phase is to maximize the effectiveness of the facility to achieve the first two objectives, above. The mass hierarchy determination and the precision determination of θ_{23} will most likely be complete in the first phase of LBNE; while the precision determination of CP violation will require the full-scope LBNE, an initial measurement of the CP phase parameter $\delta_{\rm CP}$ will be performed in earlier phases.

Secondary objectives, which may also be enabled by the facility designed to achieve the primary objectives, include:

1. other accelerator-based, neutrino oscillation measurements; these could include further sensitivity to Beyond Standard Model (BSM) physics such as nonstandard interactions

2. measurements of neutrino oscillation phenomena using atmospheric neutrinos

3. measurement of other astrophysical phenomena using medium-energy neutrinos

Additional secondary objectives, the achievement of which may require upgrades to the facility that is designed to achieve the primary physics objectives (e.g., deployment of additional detector mass or alternate detector technologies), include:

1. detection and measurement of the diffuse supernova-neutrino flux
2. measurements of neutrino oscillation phenomena and of solar physics using solar neutrinos
3. measurements of astrophysical and geophysical neutrinos of low energy

In addition, a rich set of science objectives enabled by a sophisticated near neutrino detector have been identified. A primary and a secondary objective, respectively, are:

1. measurements necessary to achieve the primary physics research objectives listed above
2. studies of neutrino interactions that may be enabled either by the facility designed to achieve the primary objectives or by future upgrades to the facility and detectors; these include precision studies of the weak interaction, studies of nuclear and nucleon structure, and searches for new physics

2.2 Neutrino Three-Flavor Mixing, CP Violation and the Mass Hierarchy

The Standard Model of particle physics (Figure 2.1) presents a remarkably accurate description of the elementary particles and their interactions. However, its limitations beg deeper questions about Nature. The unexplained patterns of quarks, leptons, flavors and generations imply that a more fundamental underlying theory must exist. LBNE plans to pursue a detailed study of neutrino mixing, resolve the neutrino mass ordering, and search for CP violation in the lepton sector by studying the oscillation patterns of high-intensity ν_μ and $\overline{\nu}_\mu$ beams measured over a long baseline.

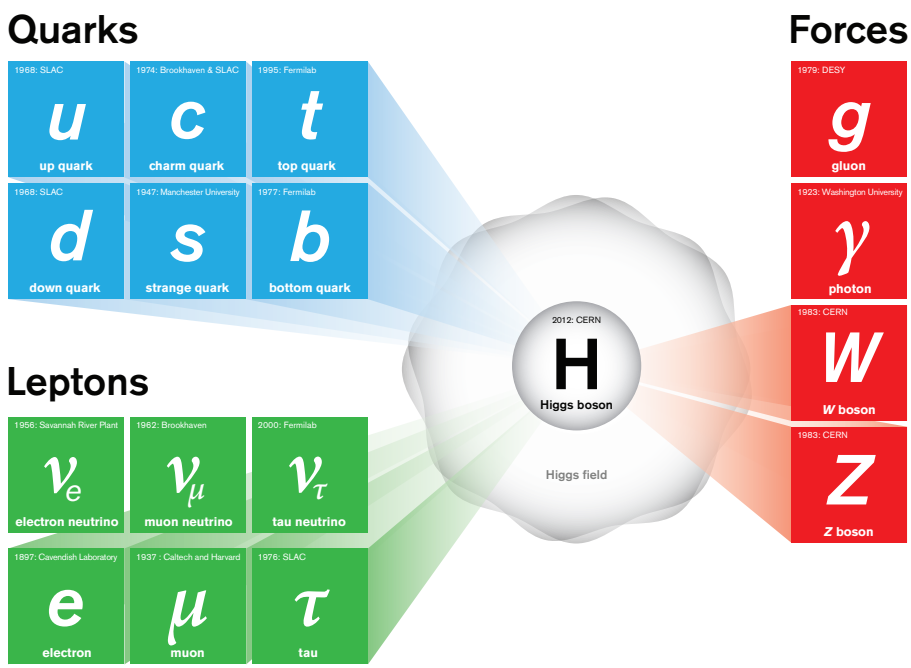

Figure 2.1: Known particles and forces in the Standard Model of particle physics. The quarks and leptons are arranged in pairs into three generations: $(u, d), (c, s), (t, b)$ and $(\nu_e, e), (\nu_\mu, \mu), (\nu_\tau, \tau)$, respectively. There are three known neutrino mass states ν_1, ν_2, ν_3 which are mixtures of the three neutrino flavors ν_e, ν_μ, ν_τ shown in this figure. The Standard Model includes the gluon (g), photon (γ) and $(W^\pm, Z^0)$ bosons that are the mediators of the strong, electromagnetic and weak interactions, respectively. The Higgs boson is a manifestation of the Higgs field that endows all the known particles with mass.

Results from the last decade, indicating that the three known types of neutrinos have nonzero mass, mix with one another and oscillate between generations, imply physics beyond the Standard Model [2]. Each of the three flavors of neutrinos, ν_e, ν_μ and ν_τ (Figure 2.1), is known to be a different mix of three mass eigenstates ν_1, ν_2 and ν_3 (Figure 2.2). In the Standard Model, the simple Higgs mechanism, which has now been confirmed by the observation of the Higgs boson [3,4], is responsible for both quark and lepton masses, mixing and charge-parity (CP) violation (the mechanism responsible for matter-antimatter asymmetries). However, the small size of neutrino masses and their relatively large mixing bears little resemblance to quark masses and mixing, suggesting that different physics — and possibly different mass scales — in the two sectors may be present, and motivating precision study of mixing and CP violation in the lepton sector.

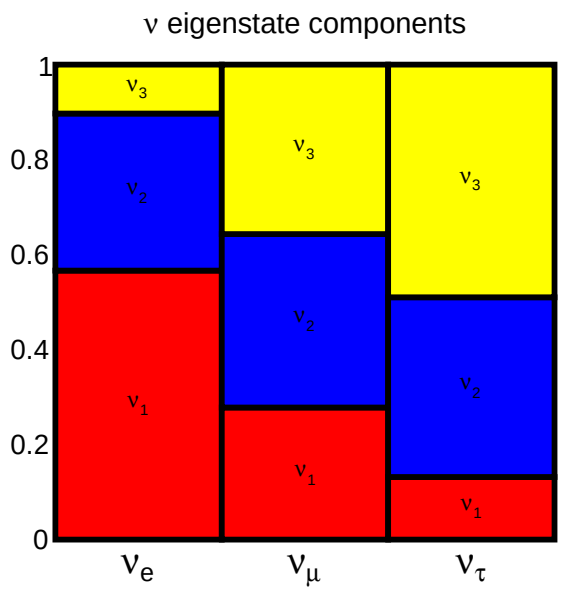

Figure 2.2: The neutrino mass eigenstate components of the known flavor eigenstates.

Neutrino oscillation arises from mixing between the flavor and mass eigenstates of neutrinos, corresponding to the weak and gravitational interactions, respectively. This three-flavor-mixing scenario can be described by a rotation between the weak-interaction eigenstate basis $(\nu_e,\ \nu_\mu,\ \nu_\tau)$ and the basis of states of definite mass $(\nu_1,\ \nu_2,\ \nu_3)$. In direct correspondence with mixing in the quark sector, the transformations between basis states is expressed in the form of a complex unitary matrix, known as the PMNS matrix :

$$\begin{pmatrix} \nu_e \\ \nu_\mu \\ \nu_\tau \end{pmatrix} = \underbrace{\begin{pmatrix} U_{e1} & U_{e2} & U_{e3} \\ U_{\mu 1} & U_{\mu 2} & U_{\mu 3} \\ U_{\tau 1} & U_{\tau 2} & U_{\tau 3} \end{pmatrix}}_{U_{\mathrm{PMNS}}} \begin{pmatrix} \nu_1 \\ \nu_2 \\ \nu_3 \end{pmatrix}. \tag{2.1}$$

The PMNS matrix in full generality depends on just three mixing angles and a CP-violating phase. The mixing angles and phase are designated as $(\theta_{12},\, \theta_{23},\, \theta_{13})$ and δ_{CP}. This matrix can be parameterized as the product of three two-flavor mixing matrices as follows, where $c_{\alpha\beta} = \cos\theta_{\alpha\beta}$ and $s_{\alpha\beta} = \sin\theta_{\alpha\beta}$:

$$U_{\mathrm{PMNS}} = \underbrace{\begin{pmatrix} 1 & 0 & 0 \\ 0 & c_{23} & s_{23} \\ 0 & -s_{23} & c_{23} \end{pmatrix}}_{\mathrm{I}} \underbrace{\begin{pmatrix} c_{13} & 0 & e^{i\delta_{\mathrm{CP}}} s_{13} \\ 0 & 1 & 0 \\ -e^{i\delta_{\mathrm{CP}}} s_{13} & 0 & c_{13} \end{pmatrix}}_{\mathrm{II}} \underbrace{\begin{pmatrix} c_{12} & s_{12} & 0 \\ -s_{12} & c_{12} & 0 \\ 0 & 0 & 1 \end{pmatrix}}_{\mathrm{III}} \tag{2.2}$$

The parameters of the PMNS matrix determine the probability amplitudes of the neutrino oscillation phenomena that arise from mixing.

The relationship between the three mixing angles θ_{12}, θ_{23}, and θ_{13} and the mixing between the neutrino flavor and mass states can be described as follows [5]:

$$\tan^2\theta_{12} \;:\; \frac{\text{amount of } \nu_{\mathrm{e}} \text{ in } \nu_2}{\text{amount of } \nu_{\mathrm{e}} \text{ in } \nu_1} \tag{2.3}$$

$$\tan^2\theta_{23} \;:\; \text{ratio of } \nu_\mu \text{ to } \nu_\tau \text{ in } \nu_3 \tag{2.4}$$

$$\sin^2\theta_{13} \;:\; \text{amount of } \nu_{\mathrm{e}} \text{ in } \nu_3 \tag{2.5}$$

The frequency of neutrino oscillation among the weak-interaction (flavor) eigenstates depends on the difference in the squares of the neutrino masses, $\Delta m^2_{ij} \equiv m_i^2 - m_j^2$; a set of three neutrino mass states implies two independent mass-squared differences (Δm^2_{21} and Δm^2_{32}). The ordering of the mass states is known as the *neutrino mass hierarchy*. An ordering of $m_1 < m_2 < m_3$ is known as the *normal hierarchy* since it matches the ordering of the quarks in the Standard Model, whereas an ordering of $m_3 < m_1 < m_2$ is referred to as the *inverted hierarchy*.

Since each flavor eigenstate is a mixture of three mass eigenstates, there can be an overall phase difference between the quantum states, referred to as δ_{CP}. A nonzero value of this phase implies that neutrinos and antineutrinos oscillate differently — a phenomenon known as charge-parity (CP) violation. δ_{CP} is therefore often referred to as the *CP phase* or the *CP-violating phase*.

The entire complement of neutrino experiments to date has measured five of the mixing parameters: the three angles θ_{12}, θ_{23} and (recently) θ_{13}, and the two mass differences Δm^2_{21} and Δm^2_{32}. The sign of Δm^2_{21} is known, but not that of Δm^2_{32}, which is the crux of the mass hierarchy ambiguity. The values of θ_{12} and θ_{23} are large, while θ_{13} is smaller [6]. The value of δ_{CP} is unknown. The real values of the entries of the PMNS mixing matrix, which contains information on the strength of

flavor-changing weak decays in the lepton sector, can be expressed in approximate form as

$$|U_{\mathrm{PMNS}}| \sim \begin{pmatrix} 0.8 & 0.5 & 0.2 \\ 0.5 & 0.6 & 0.6 \\ 0.2 & 0.6 & 0.8 \end{pmatrix}. \tag{2.6}$$

The three-flavor-mixing scenario for neutrinos is now well established. However, the mixing parameters are not known to the same precision as are those in the corresponding quark sector, and several important quantities, including the value of δ_{CP} and the sign of the large mass splitting, are still undetermined. In addition, several recent anomalous experimental results count among their possible interpretations phenomena that do not fit this model [7,8,9,10].

The relationships between the values of the parameters in the neutrino and quark sectors suggest that mixing in the two sectors is qualitatively different. Illustrating this difference, the value of the entries of the CKM quark-mixing matrix (analogous to the PMNS matrix for neutrinos, and thus indicative of the strength of flavor-changing weak decays in the quark sector) can be expressed in approximate form as

$$|V_{\mathrm{CKM}}| \sim \begin{pmatrix} 1 & 0.2 & 0.004 \\ 0.2 & 1 & 0.04 \\ 0.008 & 0.04 & 1 \end{pmatrix} \tag{2.7}$$

and compared to the entries of the PMNS matrix given in Equation 2.6. As discussed in [11], the question of why the quark mixing angles are smaller than the lepton mixing angles is an important part of the "flavor problem."

Quoting the discussion in [12], "while the CKM matrix is almost proportional to the identity matrix plus hierarchically ordered off-diagonal elements, the PMNS matrix is far from diagonal and, with the possible exception of the U_{e3} element, all elements are $\mathcal{O}(1)$." One theoretical method often used to address this question involves the use of non-Abelian discrete subgroups of $SU(3)$ as flavor symmetries; the popularity of this method comes partially from the fact that these symmetries can give rise to the nearly *tri-bi-maximal** structure of the PMNS matrix. Whether employing these flavor symmetries or other methods, any theoretical principle that attempts to describe the fundamental symmetries implied by the observed organization of quark and neutrino mixing — such as those proposed in unification models — leads to testable predictions such as sum rules between CKM and PMNS parameters [12,2,11,14]. Data on the patterns of neutrino mixing are already proving crucial in the quest for a relationship between quarks and leptons and their seemingly arbitrary generation structure. Table 2.1 displays the comparison between quark and lepton mixing

*Tri-bi-maximal mixing refers to a form of the neutrino mixing matrix with effective bimaximal mixing of ν_μ and ν_τ at the atmospheric scale ($L/E \sim 500$ km/ GeV) and effective trimaximal mixing for ν_e with ν_μ and ν_τ at the solar scale ($L/E \sim 15{,}000$ km/ GeV) [13].

in terms of the fundamental parameters and the precision to which they are known†, highlighting the limited precision of the neutrino-mixing parameter measurements.

Table 2.1: Best-fit values of the neutrino mixing parameters in the PMNS matrix (assumes normal hierarchy) from [15], their 1σ uncertainties and comparison to the analogous values in the CKM matrix [16]. ΔM^2 is defined as $m_3^2 - (m_1^2 + m_2^2)/2$.

Parameter	Value (neutrino PMNS matrix)	Value (quark CKM matrix)
$\boldsymbol{\theta_{12}}$	$34 \pm 1^\circ$	$13.04 \pm 0.05^\circ$
$\boldsymbol{\theta_{23}}$	$38 \pm 1^\circ$	$2.38 \pm 0.06^\circ$
$\boldsymbol{\theta_{13}}$	$8.9 \pm 0.5^\circ$	$0.201 \pm 0.011^\circ$
$\boldsymbol{\Delta m^2_{21}}$	$+(7.54 \pm 0.22) \times 10^{-5}$ eV^2	
$\boldsymbol{\lvert\Delta M^2\rvert}$	$(2.43^{+0.10}_{-0.06}) \times 10^{-3}$ eV^2	$m_3 >> m_2$
$\boldsymbol{\delta_{\mathrm{CP}}}$	$-170 \pm 54^\circ$	$67 \pm 5^\circ$

Clearly much work remains in order to complete the standard three-flavor mixing picture, particularly with regard to θ_{23} (is it less than, greater than, or equal to 45°?), mass hierarchy (normal or inverted?) and δ_{CP}. Additionally, there is great value in obtaining a set of measurements for multiple parameters *from a single experiment*, so that correlations and systematic uncertainties can be handled properly. Such an experiment would also be well positioned to extensively test the standard picture of three-flavor mixing. LBNE is designed to be this experiment.

2.2.1 CP Violation in the Quark and Lepton Sectors

In the particular parameterization of the PMNS matrix shown in Equation 2.2, the middle factor, labeled 'II', describes the mixing between the ν_1 and ν_3 mass states, and depends on the CP-violating phase δ_{CP}. In the three-flavor model, leptonic CP violation in an oscillation mode occurs due to the interference of contributions from terms in this factor — some of which contain δ_{CP} (i.e., involve the ν_1-ν_3 mixing directly) and some of which do not. The presence of nonzero CP-odd terms, e.g., Equation 2.15, (which requires $\delta_{\mathrm{CP}} \neq 0$ or π) in the interference patterns would result in an asymmetry in neutrino versus antineutrino oscillations. The magnitude of the CP-violating terms in the oscillation depends most directly on the size of the Jarlskog Invariant [17], a function that was introduced to provide a measure of CP violation independent of mixing-matrix parameterization. In terms of the three mixing angles and the (as yet unmeasured) CP-violating phase, the Jarlskog Invariant is:

$$J_{CP}^{\mathrm{PMNS}} \equiv \frac{1}{8} \sin 2\theta_{12} \sin 2\theta_{13} \sin 2\theta_{23} \cos\theta_{13} \sin\delta_{\mathrm{CP}}. \tag{2.8}$$

†A global fit [15] to existing results from current experiments sensitive to neutrino oscillation effects is the source for the PMNS matrix values.

The relatively large values of the mixing angles in the lepton sector imply that leptonic CP-violation effects may be quite large — depending on the value of the phase $\delta_{\rm CP}$, which is currently unknown. Experimentally, it is unconstrained at the 2σ level by the global fit [15]. Many theoretical models, examples of which include [18,19,20,21,22,23], provide predictions for $\delta_{\rm CP}$, but these predictions range over all possible values so do not yet provide any guidance.

Given the current best-fit values of the mixing angles [15] and assuming normal hierarchy,

$$J_{CP}^{\rm PMNS} \approx 0.03 \sin \delta_{\rm CP}. \tag{2.9}$$

This is in sharp contrast to the very small mixing in the quark sector, which leads to a very small value of the corresponding quark-sector Jarlskog Invariant [16],

$$J_{CP}^{\rm CKM} \approx 3 \times 10^{-5}, \tag{2.10}$$

despite the large value of $\delta_{CP}^{\rm CKM} \approx 70^\circ$.

To date, all observed CP-violating effects have occurred in experiments involving systems of quarks, in particular strange and b-mesons [16]. Furthermore, in spite of several decades of experimental searches for other sources of CP violation, all of these effects are explained by the CKM quark-mixing paradigm, and all are functions of the quark-sector CP phase parameter, $\delta_{\rm CP}^{\rm CKM}$. In cosmology, successful synthesis of the light elements after the Big Bang [24,25] (Big Bang Nucleosynthesis) requires that there be an imbalance in the number of baryons and antibaryons to one part in a billion when the Universe is a few minutes old [26]. CP violation in the quark sector has not, however, been able to explain the observed Baryon Asymmetry of the Universe (BAU), due to the small value of J_{CP}^{CKM}.

Baryogenesis [27] is a likely mechanism for generating the observed matter-antimatter asymmetry of our Universe. One way that it is elegantly achieved is by first having *leptogenesis* in the very early Universe. That mechanism can come about from the production and decay of very heavy right-handed neutrinos, if they are Majorana states (i.e. do not conserve lepton number[‡]), CP symmetry is violated in their decays (thus distinguishing particles and antiparticles) and the Universe is in non-equilibrium. Leptogenesis will lead to an early dominance of antileptons over leptons. When the cooling Universe reaches the electroweak phase transition, $T \sim 250\,$GeV, a baryon number excess is generated from the lepton asymmetry by a $B - L$[‡] conserving mechanism (analogous to proton decay in that it violates B and L separately but conserves $B - L$) already present in the Standard Model.

The heavy Majorana right-handed neutrino states that could give rise to leptogenesis in the very early Universe are also a natural consequence of the GUT-based *seesaw* mechanism [28] — the simplest and most natural explanation of the observed super-light neutrino mass scales. The seesaw

[‡]In the Standard Model, lepton number (L) and baryon number (B) are conserved quantum numbers. Leptons have $B = 0$ and $L = 1$ and antileptons have $L = -1$. A quark has $L = 0$ and $B = 1/3$ and an antiquark has $B = -1/3$.

mechanism is a theoretical attempt to reconcile the very small masses of neutrinos to the much larger masses of the other elementary particles in the Standard Model. The seesaw mechanism achieves this unification by assuming an unknown new physics scale that connects the observed low-energy neutrino masses with a higher mass scale that involves very heavy sterile neutrino states. The seesaw mechanism as generator of neutrino mass is in addition to the Higgs mechanism that is now known to be responsible for the generation of the quark, charged lepton, and vector boson masses.

The no-equilibrium leptogenesis ingredient is expected in a hot Big Bang scenario, but the Majorana nature of the heavy neutrinos and needed CP violation can only be indirectly inferred from light neutrino experiments by finding lepton number violation (validating their Majorana nature via neutrinoless double-beta decay) and observing CP violation in ordinary neutrino oscillations.

Recent theoretical advances have demonstrated that CP violation, necessary for the generation of the Baryon Asymmetry of the Universe at the GUT scale (baryogenesis), can be directly related to the low-energy CP violation in the lepton sector that could manifest in neutrino oscillations. As an example, the theoretical model described in [29] predicts that leptogenesis, the generation of the analogous lepton asymmetry, can be achieved if

$$|\sin\theta_{13}\sin\delta_{\rm CP}| \gtrsim 0.11 \tag{2.11}$$

This implies $|\sin\delta_{\rm CP}| \gtrsim 0.7$ given the latest global fit value of $|\sin\theta_{13}|$ [30].

The goal of establishing an experimental basis for assessing this possibility should rank very high on the list of programmatic priorities within particle physics, and can be effectively addressed by LBNE.

2.2.2 Observation of CP-Violating Effects in Neutrino Oscillation Experiments

Whereas the Standard Model allows for violation of charge-parity (CP) symmetries in weak interactions, CP transformations followed by time-reversal transformations (CPT) are invariant. Under CPT invariance, the probabilities of neutrino oscillation and antineutrino oscillation are equivalent, i.e., $P(\nu_l \to \nu_l) = P(\overline{\nu}_l \to \overline{\nu}_l)$ where $l = e,\ \mu,\ \tau$. Measurements of $\nu_l \to \nu_l$ oscillations in which the flavor of the neutrino before and after oscillations remains the same are referred to as *disappearance* or *survival* measurements. CPT invariance in neutrino oscillations was recently tested by measurements of $\nu_\mu \to \nu_\mu$ and $\overline{\nu}_\mu \to \overline{\nu}_\mu$ oscillations [31]; no evidence for CPT violation was found. Therefore, asymmetries in neutrino versus antineutrino oscillations arising from CP violation effects can only be accessed in *appearance* experiments, defined as oscillations of $\nu_l \to \nu_{l'}$, in

which the flavor of the neutrino after oscillations has changed. Because of the intrinsic challenges of producing and detecting ν_τ's, the oscillation modes $\nu_{\mu,e} \to \nu_{e,\mu}$ provide the most promising experimental signatures of leptonic CP violation.

For $\nu_{\mu,e} \to \nu_{e,\mu}$ oscillations that occur as the neutrinos propagate through matter, as in terrestrial long-baseline experiments, the coherent forward scattering of ν_e's on electrons in matter modifies the energy and path-length dependence of the vacuum oscillation probability in a way that depends on the magnitude *and* sign of Δm^2_{32}. This is the Mikheyev-Smirnov-Wolfenstein (MSW) effect [32,33] that has already been observed in solar-neutrino oscillation (disappearance) experiments [34,35,36,37]. The oscillation probability of $\nu_{\mu,e} \to \nu_{e,\mu}$ through matter, in a constant density approximation, keeping terms up to second order in $\alpha \equiv |\Delta m^2_{21}|/|\Delta m^2_{31}|$ and $\sin^2\theta_{13}$, is [38,16]:

$$P(\nu_\mu \to \nu_e) \cong P(\nu_e \to \nu_\mu) \cong P_0 + \underbrace{P_{\sin\delta}}_{\text{CP violating}} + P_{\cos\delta} + P_3 \tag{2.12}$$

where

$$P_0 = \sin^2\theta_{23}\frac{\sin^2 2\theta_{13}}{(A-1)^2}\sin^2[(A-1)\Delta], \tag{2.13}$$

$$P_3 = \alpha^2\cos^2\theta_{23}\frac{\sin^2 2\theta_{12}}{A^2}\sin^2(A\Delta), \tag{2.14}$$

$$P_{\sin\delta} = \alpha\frac{8J_{cp}}{A(1-A)}\sin\Delta\sin(A\Delta)\sin[(1-A)\Delta], \tag{2.15}$$

$$P_{\cos\delta} = \alpha\frac{8J_{cp}\cot\delta_{\rm CP}}{A(1-A)}\cos\Delta\sin(A\Delta)\sin[(1-A)\Delta], \tag{2.16}$$

and where

$$\Delta = \Delta m^2_{31}L/4E,\ and\ A = \sqrt{3}G_F N_e 2E/\Delta m^2_{31}.$$

In the above, the CP phase $\delta_{\rm CP}$ appears (via J_{cp}) in the expressions for $P_{\sin\delta}$ (the CP-odd term) which switches sign in going from $\nu_\mu \to \nu_e$ to the $\overline{\nu}_\mu \to \overline{\nu}_e$ channel, and $P_{\cos\delta}$ (the CP-conserving term) which does not. The matter effect also introduces a neutrino-antineutrino asymmetry, the origin of which is simply the presence of electrons and absence of positrons in the Earth.

Recall that in Equation 2.2, the CP phase appears in the PMNS matrix through the mixing of the ν_1 and ν_3 mass states. The physical characteristics of an appearance experiment are therefore determined by the baseline and neutrino energy at which the mixing between the ν_1 and ν_3 states is maximal, as follows:

$$\frac{L(\text{km})}{E_\nu(\text{GeV})} = (2n-1)\frac{\pi}{2}\frac{1}{1.27\times\Delta m^2_{31}(\text{eV}^2)} \tag{2.17}$$

$$\approx (2n-1)\times 510\ \text{km/GeV} \tag{2.18}$$

where $n = 1, 2, 3...$ denotes the oscillation nodes at which the appearance probability is maximal.

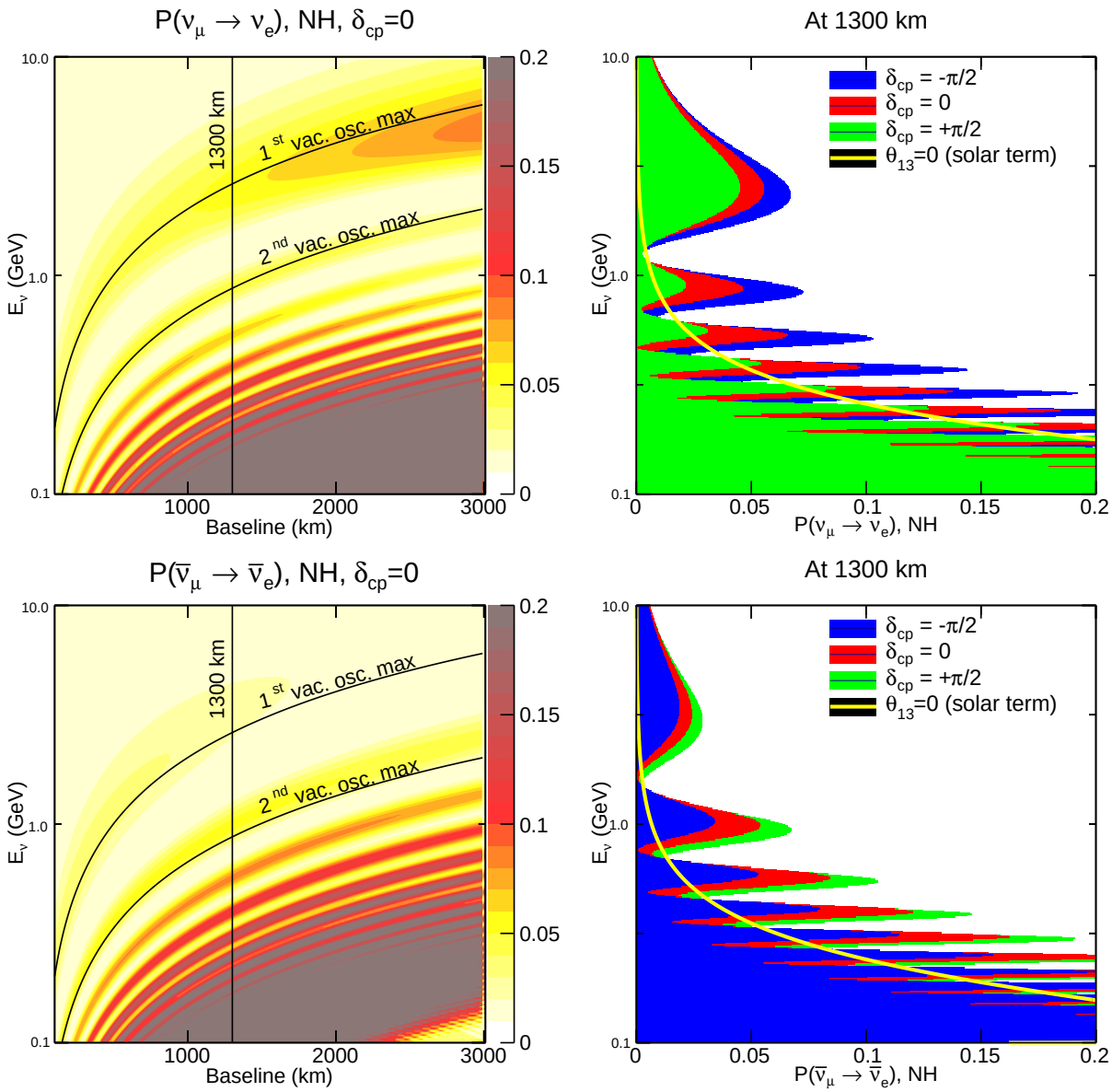

Figure 2.3: Neutrino oscillation probabilities as a function of energy and baseline, for different values of $\delta_{\rm CP}$, *normal hierarchy*. The oscillograms on the left show the $\nu_\mu \to \nu_e$ oscillation probabilities as a function of baseline and energy for *neutrinos* (top left) and *antineutrinos* (bottom left) with $\delta_{\rm CP} = 0$. The figures on the right show the projection of the oscillation probability on the neutrino energy axis at a baseline of 1,300 km for $\delta_{\rm CP} = 0$ (red), $\delta_{\rm CP} = +\pi/2$ (green), and $\delta_{\rm CP} = -\pi/2$ (blue) for neutrinos (top right) and antineutrinos (bottom right). The yellow curve is the ν_e appearance solely from the "solar term" due to ν_1 to ν_2 mixing as given by Equation 2.14.

The dependences on E_ν of the oscillation probability for the LBNE baseline of L =1,300 km are plotted on the right in Figures 2.3 and 2.4. The colored curves demonstrate the variation in the ν_e appearance probability as a function of E_ν, for three different values of $\delta_{\rm CP}$.

The variation in the $\nu_\mu \to \nu_e$ oscillation probabilities with the value of $\delta_{\rm CP}$ indicates that it is

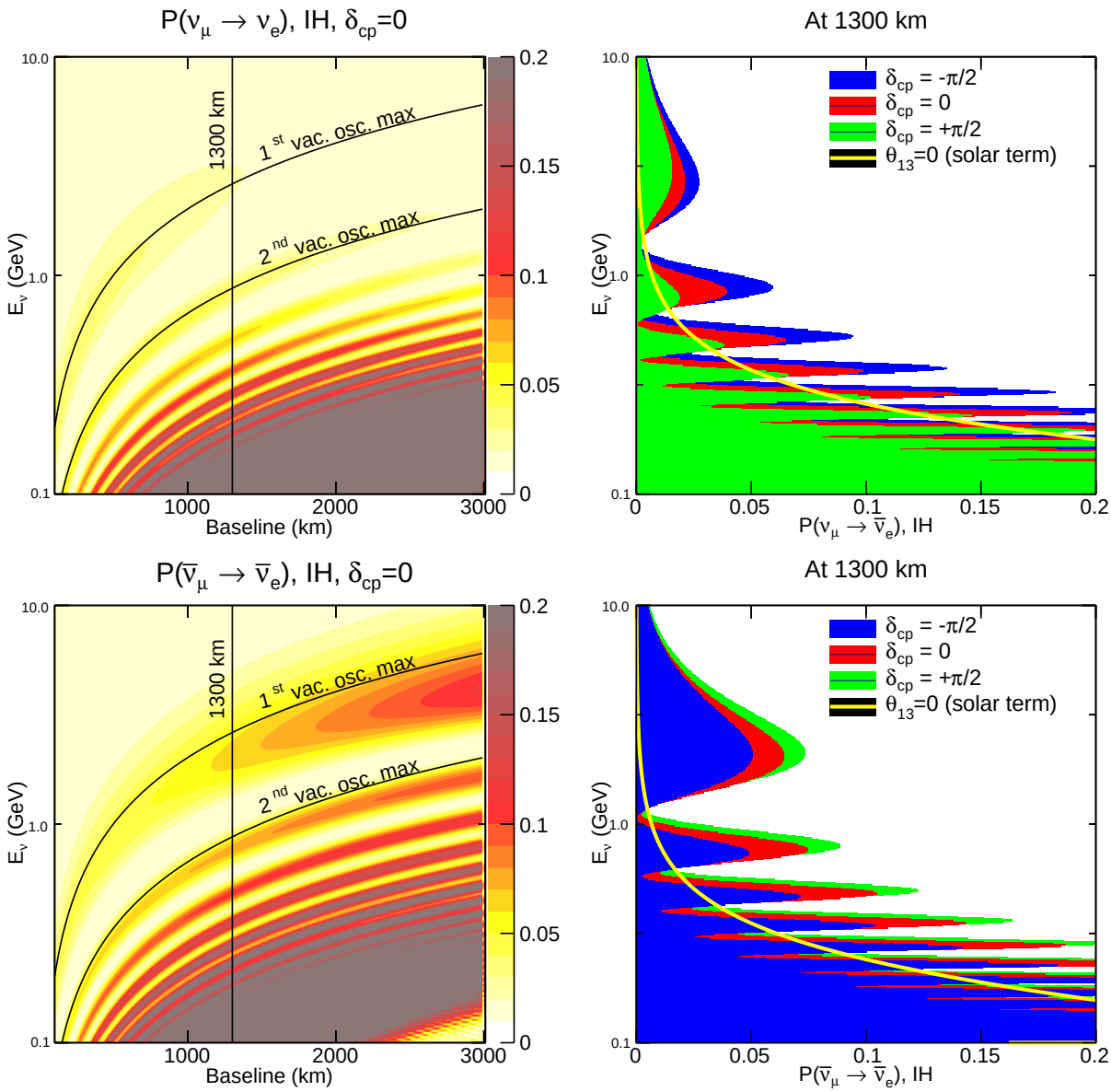

Figure 2.4: Neutrino oscillation probabilities as a function of energy and baseline, for different values of $\delta_{\rm CP}$, *inverted hierarchy*. The oscillograms on the left show the $\nu_\mu \to \nu_e$ oscillation probabilities as a function of baseline and energy for *neutrinos* (top left) and *antineutrinos* (bottom left) with $\delta_{\rm CP} = 0$. The figures on the right show the projection of the oscillation probability on the neutrino energy axis at a baseline of 1,300 km for $\delta_{\rm CP} = 0$ (red), $\delta_{\rm CP} = +\pi/2$ (green), and $\delta_{\rm CP} = -\pi/2$ (blue) for neutrinos (top right) and antineutrinos (bottom right).The yellow curve is the ν_e appearance solely from the "solar term" due to ν_1 to ν_2 mixing as given by Equation 2.14.

experimentally possible to measure the value of $\delta_{\rm CP}$ at a fixed baseline using only the observed shape of the $\nu_\mu \to \nu_e$ *or* the $\overline{\nu}_\mu \to \overline{\nu}_e$ appearance signal measured over an energy range that encompasses at least one full oscillation interval. A measurement of the value of $\delta_{\rm CP} \neq 0$ or π, assuming that neutrino mixing follows the three-flavor model, would imply CP violation. The CP

asymmetry, $\mathcal{A}_{CP}$, is defined as

$$\mathcal{A}_{CP} = \frac{P(\nu_\mu \to \nu_e) - P(\overline{\nu}_\mu \to \overline{\nu}_e)}{P(\nu_\mu \to \nu_e) + P(\overline{\nu}_\mu \to \overline{\nu}_e)}. \tag{2.19}$$

In the three-flavor model the asymmetry can be approximated to leading order in Δm^2_{21} as [39]:

$$\mathcal{A}_{CP} \sim \frac{\cos\theta_{23}\sin 2\theta_{12}\sin\delta_{\rm CP}}{\sin\theta_{23}\sin\theta_{13}}\left(\frac{\Delta m^2_{21}L}{4E_\nu}\right) + \text{matter effects} \tag{2.20}$$

Regardless of the value obtained for $\delta_{\rm CP}$, it is clear that the explicit observation of an asymmetry between $P(\nu_l \to \nu_{l'})$ and $P(\overline{\nu}_l \to \overline{\nu}_{l'})$ is sought to directly demonstrate the leptonic CP violation effect that a value of $\delta_{\rm CP}$ different from zero or π implies. For long-baseline experiments such as LBNE, where the neutrino beam propagates through the Earth's mantle, the leptonic CP-violation effects must be disentangled from the matter effects.

2.2.3 Probing the Neutrino Mass Hierarchy via the Matter Effect

The asymmetry induced by matter effects as neutrinos pass through the Earth arises from the change in sign of the factors proportional to Δm^2_{31} (namely A, Δ and α; Equations 2.12 to 2.16) in going from the normal to the inverted neutrino mass hierarchy. This sign change provides a means for determining the currently unknown mass hierarchy. The oscillation probabilities given in these approximate equations for $\nu_\mu \to \nu_e$ as a function of baseline in kilometers and energy in GeV are calculated numerically with an exact formalism [40] and shown in the oscillograms of Figure 2.3 and 2.4 for $\delta_{\rm CP} = 0$, for normal and inverted hierarchies, respectively. The oscillograms include the matter effect, assuming an Earth density and electron fraction described by [41]. These values are taken as a constant average over paths through regions of the Earth with continuous density change. Any baseline long enough to pass through a discontinuity is split into three or more segments each of constant average density and electron fraction. The solid black curves in the oscillograms indicate the location of the first and second oscillation maxima as given by Equation 2.18, assuming oscillations in a vacuum; matter effects will change the neutrino energy values at which the mixing between the ν_1 and ν_3 mass states is maximal.

The significant impact of the matter effect on the $\nu_\mu \to \nu_e$ and $\overline{\nu}_\mu \to \overline{\nu}_e$ oscillation probabilities at longer baselines (Figures 2.3 and 2.4) implies that ν_e appearance measurements over long distances through the Earth provide a powerful probe into the neutrino mass hierarchy question: is $m_1 > m_3$ or vice-versa?

The dependence of the matter effect on the mass hierarchy is illustrated in the oscillograms plotted on the left hand side of Figures 2.3 and 2.4, and can be characterized as follows:

- For normal hierarchy, $P(\nu_\mu \to \nu_e)$ is enhanced and $P(\overline{\nu}_\mu \to \overline{\nu}_e)$ is suppressed. The effect increases with baseline at a fixed L/E.
- For inverted hierarchy, $P(\nu_\mu \to \nu_e)$ is suppressed and $P(\overline{\nu}_\mu \to \overline{\nu}_e)$ is enhanced. The effect increases with baseline at a fixed L/E.
- The matter effect has the largest impact on the probability amplitude at the first oscillation maximum.
- The matter effect introduces a phase shift in the oscillation pattern, shifting it to a lower energy for a given baseline when the hierarchy changes from normal to inverted. The shift is approximately -100 MeV.

2.2.4 Disentangling CP-Violating and Matter Effects

In Figure 2.5, the asymmetries induced by matter and maximal CP violation (at $\delta_{\mathrm{CP}} = \pm\pi/2$) are shown separately as 2D oscillograms in baseline and neutrino energy. The matter effect induces an asymmetry in $P(\nu_l \to \nu_{l'})$ and $P(\overline{\nu}_l \to \overline{\nu}_{l'})$ that adds to the CP asymmetry. At longer baselines ($> 1000\,\mathrm{km}$), the matter asymmetry in the energy region of the first oscillation node is driven primarily by the change in the ν_e appearance amplitude. At shorter baselines ($\mathcal{O}(100\,\mathrm{km})$) the asymmetry is driven by the phase shift. The dependence of the asymmetry on baseline and energy, where the oscillation probabilities peak and the appearance signals are largest, can be approximated as follows:

$$\mathcal{A}_{cp} \propto L/E, \tag{2.21}$$

$$\mathcal{A}_{matter} \propto L \times E. \tag{2.22}$$

The phenomenology of $\nu_\mu \to \nu_e$ oscillations described in Section 2.2.2 implies that the experimental sensitivity to CP violation and the mass hierarchy from measurements of the total asymmetry between $P(\nu_l \to \nu_{l'})$ and $P(\overline{\nu}_l \to \overline{\nu}_{l'})$ requires the disambiguation of the asymmetry induced by the matter effect and that induced by CP violation. This is particularly true for experiments designed to access mixing between the ν_1 and ν_3 mass states using neutrino beams of $\mathcal{O}(1\,\mathrm{GeV})$. Such beams require baselines of at least several hundred kilometers, at which the matter asymmetries are significant. The currently known values of the oscillation parameters permit calculation of the magnitude of the matter asymmetry within an uncertainty of $< 10\%$; only the sign of the asymmetry, which depends on the sign of Δm^2_{31}, is unknown. Since the magnitude of the matter asymmetry is known, baselines at which the size of the matter asymmetry exceeds that of the maximal possible CP asymmetry are required in order to separate the two effects.

Figure 2.6 illustrates the ambiguities that can arise from the interference of the matter and CP asymmetries. The plots show the total asymmetry as a function of δ_{CP} at four baseline values (clockwise from top left): 290 km, 810 km, 2,300 km and 1,300 km. The curves in black and red

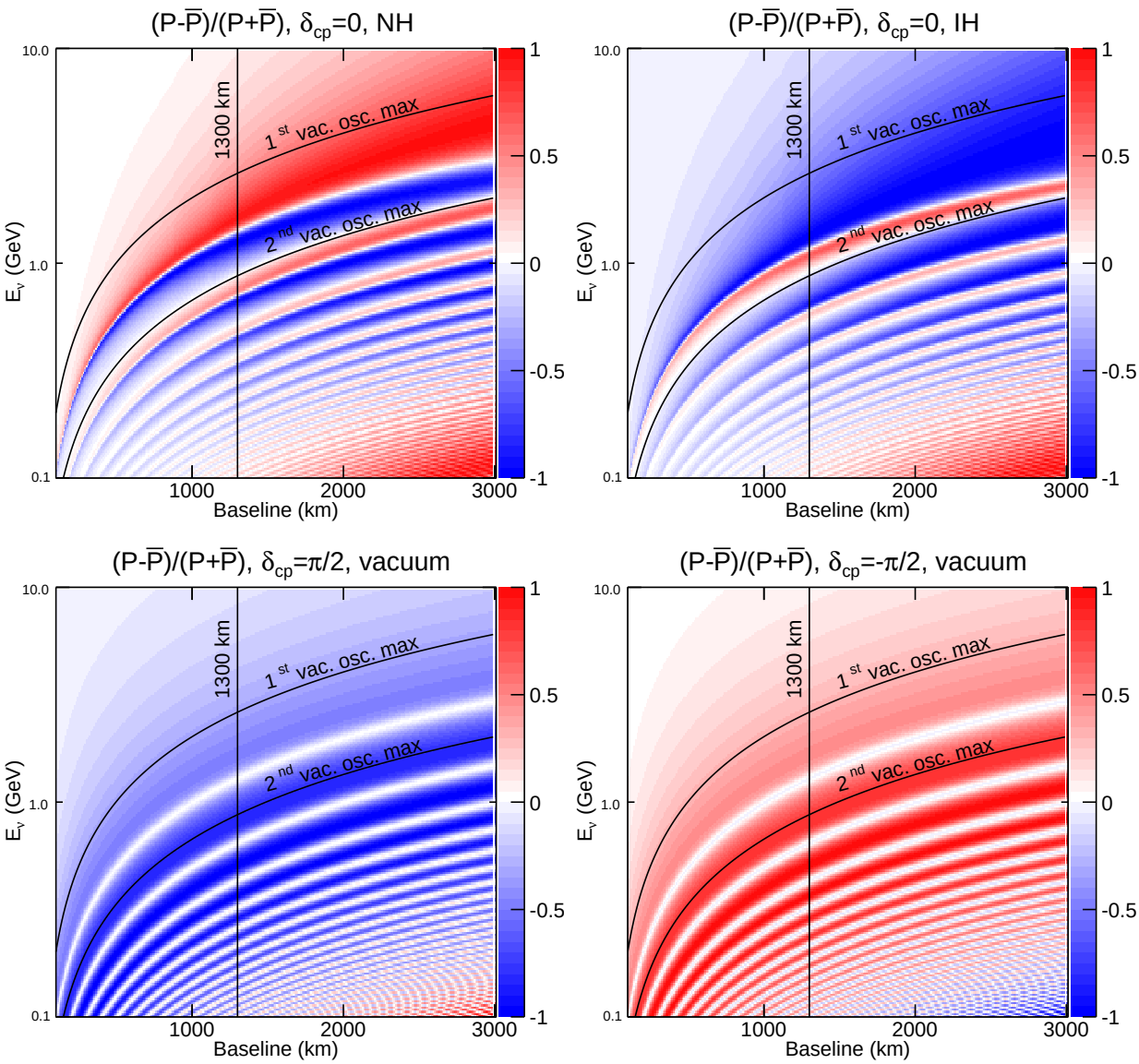

Figure 2.5: The $\nu/\overline{\nu}$ oscillation probability asymmetries as a function of baseline. The top two figures show the asymmetry induced by the matter effect only for normal (top left) and inverted (top right) hierarchies. The bottom figures show the asymmetry induced through the CP-violating phase $\delta_{\rm CP}$ in vacuum, for $\delta_{\rm CP} = +\pi/2$ (bottom left) and $\delta_{\rm CP} = -\pi/2$ (bottom right)

illustrate the asymmetries at the first and second oscillation nodes, respectively. The solid lines represent normal hierarchy, and the dashed lines represent inverted hierarchy. The plots demonstrate that experimental measurements of the asymmetry (Equation 2.19) at the first oscillation node could yield ambiguous results for short baselines if the hierarchy is unknown. This occurs in regions of the $(L, E, \delta_{\rm CP})$ phase space where the matter and CP asymmetries cancel partially or totally. For example, the green lines in Figure 2.6 indicate the asymmetry at the first node for maximal CP violation ($\delta_{\rm CP} = \pi/2$) with an inverted hierarchy. At a baseline of 290 km, the measured

asymmetry at $\delta_{\mathrm{CP}} = \pi/2$ (inverted hierarchy) is degenerate with that at $\delta_{\mathrm{CP}} \sim 0$ (normal hierarchy) at the first node. Measurements of the asymmetry at different L/E or at different baselines can break the degeneracies (Equation 2.22). At very long baselines, for which the matter asymmetry exceeds the maximal CP asymmetry at the first oscillation node, there are no degeneracies and the mass hierarchy and CP asymmetries can be resolved within the same experiment. For the current best-fit values of the oscillation parameters, the matter asymmetry exceeds the maximal possible CP asymmetry at baselines of $\geq$ 1,200 km.

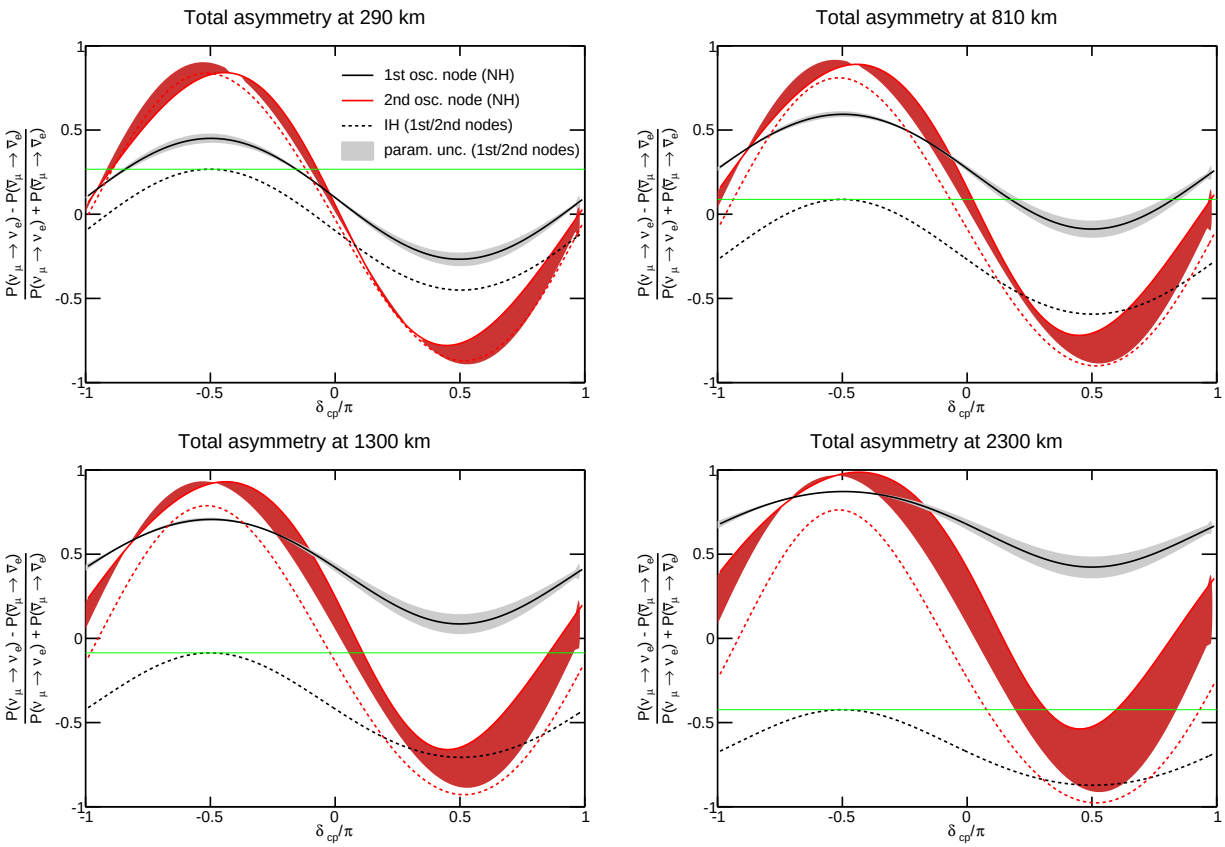

Figure 2.6: The $\nu/\overline{\nu}$ oscillation probability asymmetries versus δ_{CP} at the first two oscillation nodes. Clockwise from top left: 290 km, 810 km, 2,300 km and 1,300 km. The solid/dashed black line is the total asymmetry at the first oscillation node for normal/inverted hierarchy. The red lines indicate the asymmetries at the second node.

2.2.5 Optimization of the Oscillation Baseline for CPV and Mass Hierarchy

The simple arguments above suggest that a baseline $\geq$ 1,200 km is required to search for CP violation and determine the mass hierarchy simultaneously in a single long-baseline neutrino oscillation experiment. To understand the performance of a long-baseline experiment as a function of baseline using realistic neutrino beamline designs, a study of the sensitivities to CP violation and the mass hierarchy as a function of baseline was carried out using a neutrino beamline design optimized

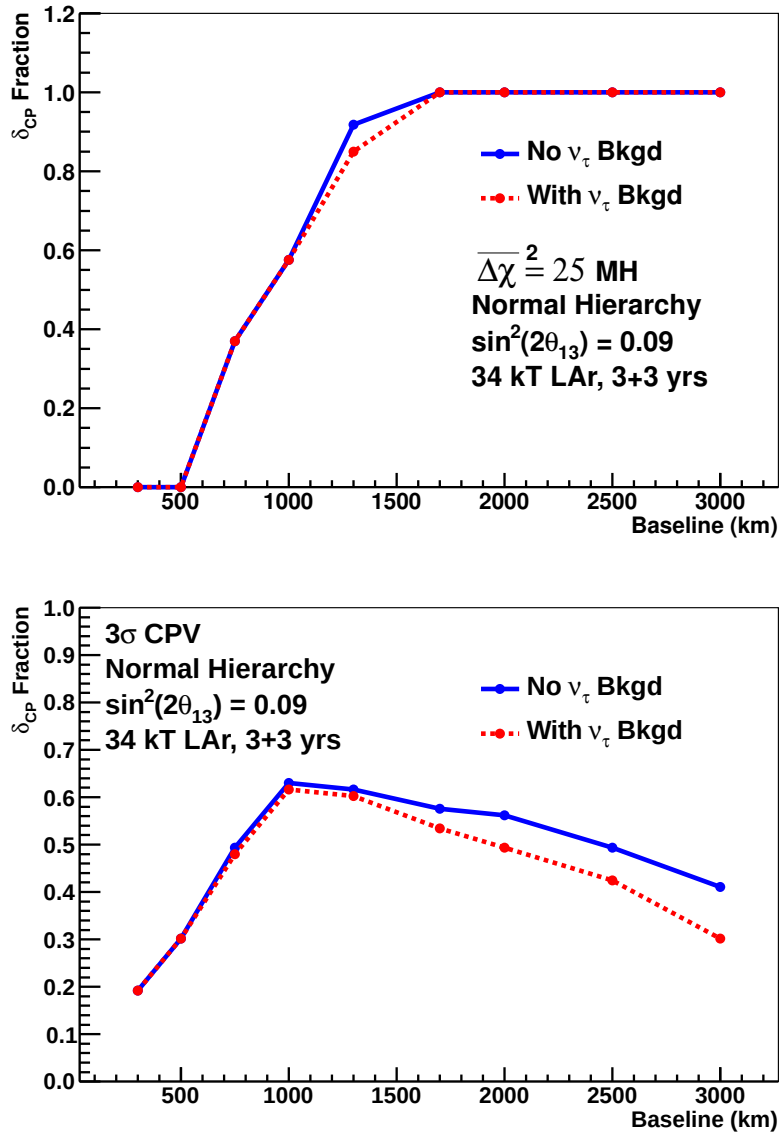

Figure 2.7: The fraction of $\delta_{\rm CP}$ values for which the mass hierarchy can be determined with an average $|\overline{\Delta\chi^2}| = 25$ or greater as a function of baseline (top) and the fraction of $\delta_{\rm CP}$ values which CP violation can be determined at the 3σ level or greater as a function of baseline (bottom). A NuMI based beam design with a 120-GeV beam was optimized for each baseline. Projections assume $\sin^2 2\theta_{13} = 0.09$ and a 34-kt LArTPC as the far detector [42]. An exposure of 3yrs+3yrs of neutrino+antineutrino running with 1.2-MW beam power is assumed.

individually for each baseline. A 34-kt LArTPC neutrino detector at the far site was assumed since it has a high ν_e-identification efficiency that is flat over a large range of energies (Chapter 4). The beamline design was based on the NuMI beamline utilizing the 120-GeV, 1.2-MW proton beam from the Fermilab Main Injector and was fully simulated using GEANT3 [43]. Varying the distance between the target and the first horn allowed selection of a beam spectrum that covered the first

oscillation node and part of the second. The design incorporated an evacuated decay pipe of 4-m diameter and a length that varied from 280 to 580 m. For baselines less than 1,000 m, the oscillation occurs at neutrino energies where on-axis beams produce too little flux. Therefore, off-axis beams — which produce narrow-band, low-energy neutrino fluxes — were simulated for these baselines, with the off-axis angle chosen to provide the most coverage of the first oscillation node. The results of this study [42] are summarized in Figure 2.7. The sensitivity to CP violation (bottom plot) assumes that the mass hierarchy is unknown. An updated study with more detail is available [44]. The baseline study indicates that with realistic experimental conditions, baselines between 1,000 and 1,300 km are near optimal for determination of CP violation. With baselines $>$ 1,500 km, the correct mass hierarchy could be determined with a probability greater than 99% for all values of δ_{CP} with a large LArTPC far detector. However, at very long baselines, in one of the neutrino beam polarities ($\nu/\overline{\nu}$ for inverted/normal hierarchy) the event rate suppression due to the matter effect becomes very large, making it difficult to observe an explicit CP-violation asymmetry.

2.2.6 Physics from Precision Measurements of Neutrino Mixing

Precision measurements of the neutrino mixing parameters in long-baseline oscillations not only reveal the neutrino mixing patterns in greater detail, but also serve as probes of new physics that manifests as perturbations in the oscillation patterns driven by three-flavor mixing.

The determination of whether there is maximal mixing between ν_μ and ν_τ — or a measurement of the deviation from maximal — is of great interest theoretically [20,45,46,47,48,49]. Models of quark-lepton universality propose that the quark and lepton mixing matrices (Equations 2.7 and 2.6, respectively) are given by

$$U^{\mathrm{CKM}} = 1 + \epsilon_{\mathrm{Cabbibo}} \text{ and} \tag{2.23}$$

$$U^{\mathrm{PMNS}} = T + \epsilon_{\mathrm{Cabbibo}}, \tag{2.24}$$

where T is determined by Majorana physics [50] and $\epsilon_{\mathrm{Cabbibo}}$ refers to small terms driven by the Cabbibo weak mixing angle ($\theta_C = \theta_{12}^{\mathrm{CKM}}$). In such models $\theta_{23} \sim \pi/4 + \Delta\theta$, where $\Delta\theta$ is of order the Cabbibo angle, θ_C, and $\theta_{13} \sim \theta_C/\sqrt{2}$. It is therefore important to determine experimentally both the value of $\sin^2\theta_{23}$ and the octant of θ_{23} if $\theta_{23} \neq 45°$.

Studying ν_μ disappearance probes $\sin^2 2\theta_{23}$ and $|\Delta m^2_{32}|$ with very high precision. Disappearance measurements can therefore determine whether ν_μ-ν_τ mixing is maximal or near maximal such that $\sin^2 2\theta_{23} = 1$, but they cannot resolve the octant of θ_{23} if ν_μ-ν_τ mixing is less than maximal. Combining the ν_μ disappearance signal with the ν_e appearance signal can help determine the θ_{23} octant and constrain some of the theoretical models of quark-lepton universality.

Direct unitarity tests, in which the individual components of the PMNS matrix are measured separately, are challenging due to limited experimentally available oscillation channels [51,52]. Application of the "proof by contradiction" principle offers another way to perform the unitarity tests. In these tests, the mixing angles are extracted from the data by assuming unitarity in the standard three-flavor framework. If measurements of the same mixing angle by two different processes are inconsistent, then the standard three-flavor framework is insufficient and new physics beyond this framework is required. Observation of unitarity violation will constrain the phase space of possible new physics. In particular, the precision measurement of $\sin^2 2\theta_{13}$ provides the most promising unitarity test [52] for the PMNS matrix. It is important to note that several theoretical models of new physics, such as the existence of sterile neutrinos or nonstandard interactions, could lead to apparent deviations of the $\sin^2 2\theta_{13}$ value measured in ν_e appearance experiments from that measured in reactor ($\overline{\nu}_e$ disappearance) experiments.

Precision measurements of ν_μ and $\overline{\nu}_\mu$ survival over long baselines could reveal nonstandard physics driven by new interactions in matter. Examples of some of these effects and the experimental signatures in long-baseline oscillations are discussed in Chapter 4.

In addition, experiments with long enough baselines and sufficient neutrino flux at $E_\nu > 3$ GeV, coupled with high-resolution tracking detectors, as in the LBNE design, can also probe $\nu_\mu \to \nu_\tau$ appearance with higher precision than is currently possible using ν_τ charged-current interactions. The combination of $\nu_\mu \to \nu_\mu$, $\nu_\mu \to \nu_e$, and $\nu_\mu \to \nu_\tau$ can ultimately over-constrain the three-flavor model of neutrino oscillations both in neutrino and antineutrino modes.

2.2.7 Oscillation Physics with Atmospheric Neutrinos

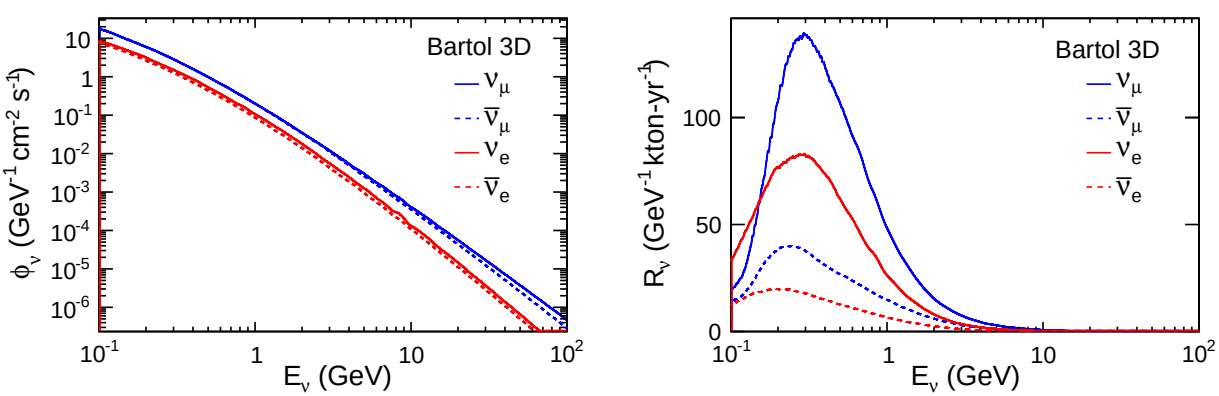

Figure 2.8: The atmospheric neutrino flux in neutrinos per second per square centimeter as a function of neutrino energy for different flavors (left). The atmospheric neutrino spectrum per GeV per kt per year for the different species (right).

Atmospheric neutrinos are unique among sources used to study oscillations; the flux contains neutrinos and antineutrinos of all flavors, matter effects play a significant role, both Δm^2 values con-

tribute to the oscillation patterns, and the oscillation phenomenology occurs over several orders of magnitude in both energy (Figure 2.8) and path length. These characteristics make atmospheric neutrinos ideal for the study of oscillations and provide a laboratory suitable to search for exotic phenomena for which the dependence of the flavor-transition and survival probabilities on energy and path length can be defined. The probabilities of atmospheric $\nu_\mu \to \nu_e$ and $\overline{\nu}_\mu \to \overline{\nu}_e$ oscillations for normal and inverted hierarchies are shown as a function of zenith angle in Figure 2.9.

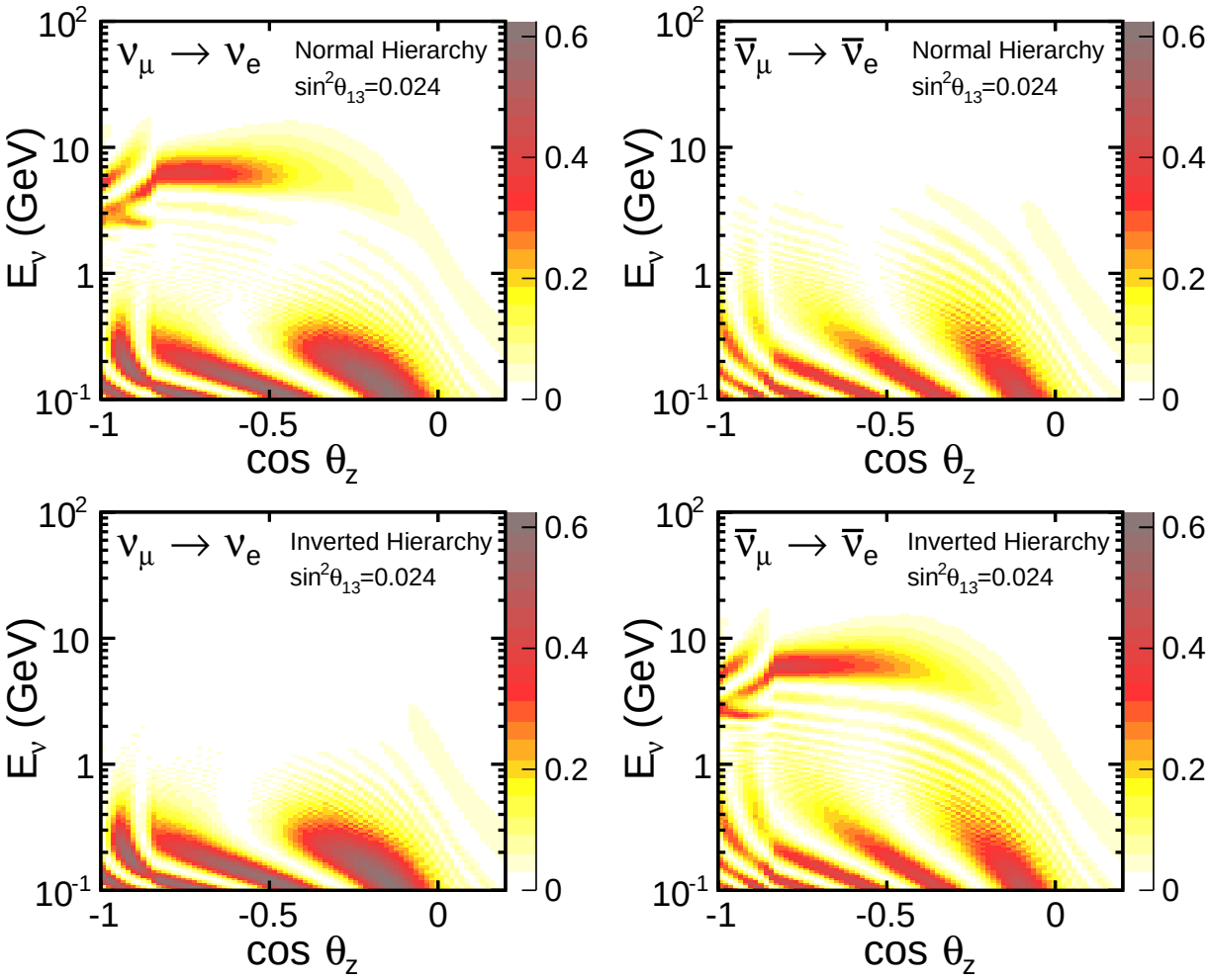

Figure 2.9: The probabilities of atmospheric $\nu_\mu \to \nu_e$ (left) and $\overline{\nu}_\mu \to \overline{\nu}_e$ (right) oscillations for normal (top) and inverted (bottom) hierarchies as a function of zenith angle.

Even with dedicated long-baseline experiments exploring the large mass splitting (Δm^2_{32}) for nearly a decade, atmospheric data continue to contribute substantially to our understanding of the neutrino sector. Broadly speaking:

- The data demonstrate *complementarity* with beam results via two- and three-flavor fits and the measurement of a ν_τ appearance signal consistent with expectations.

- The data serve to increase measurement *precision* through global fits, given that the sensitivity of atmospheric neutrinos to the mass hierarchy is largely independent of δ_{CP} and the octant of θ_{23}.

- *New physics* searches with atmospheric neutrinos have placed limits on CPT violation, non-standard interactions, mass-varying neutrinos and Lorentz-invariance violation.

Atmospheric neutrinos can continue to play these roles in the LBNE era given LBNE's deep-underground far detector. In particular, complementarity will be vital in a future where, worldwide, the number of high-precision, long-baseline beam/detector facilities is small. The physics potential of a large underground liquid argon detector for measuring atmospheric neutrinos is discussed in Section 4.6.

2.3 Nucleon Decay Physics Motivated by Grand Unified Theories

Searches for proton decay, bound-neutron decay and similar processes such as di-nucleon decay and neutron-antineutron oscillations test the apparent but unexplained conservation law of baryon number. These decays are already known to be rare based on decades of prior searches, all of which have produced negative results. If measurable event rates or even a single-candidate event were to be found, it would be sensible to presume that they occurred via unknown virtual processes based on physics beyond the Standard Model. The impact of demonstrating the existence of a baryon-number-violating process would be profound.

2.3.1 Theoretical Motivation from GUTs

The class of theories known as Grand Unified Theories (GUTs) make predictions about both baryon number violation and proton lifetime that may be within reach of the full-scope LBNE experiment. The theoretical motivation for the study of proton decay has a long and distinguished history [53,54,55] and has been reviewed many times [56,57,58]. Early GUTs provided the original motivation for proton decay searches in kiloton-scale detectors placed deep underground to limit backgrounds. The 22.5-kt Super–Kamiokande experiment extended the search for proton decay by more than an order of magnitude relative to the previous generation of experiments. Contemporary reviews [59,60,61] discuss the strict limits already set by Super–Kamiokande and the context of the proposed next generation of larger underground experiments such as Hyper-Kamiokande and LBNE.

Although no evidence for proton decay has been detected, the lifetime limits from the current generation of experiments already constrain the construction of many contemporary GUT models. In some cases, these lifetime limits are approaching the upper limits allowed by GUT models. This situation points naturally toward continuing the search with new, larger detectors. These searches are motivated by a range of scientific issues:

- Conservation laws arise from underlying symmetries in Nature [62]. Conservation of baryon number is therefore unexplained since it corresponds to no known long-range force or symmetry.
- Baryon number non-conservation has cosmological consequences, such as a role in inflation and the matter-antimatter asymmetry of the Universe.
- Proton decay is predicted at some level by almost all GUTs.
- Some GUTs can accommodate neutrinos with nonzero mass and characteristics consistent with experimental observations.
- GUTs incorporate other previously unexplained features of the Standard Model such as the relationship between quark and lepton electric charges.
- The unification scale is suggested both experimentally and theoretically by the apparent convergence of the running coupling constants of the Standard Model. The unification scale is in excess of 10^{15} GeV.
- The unification scale is not accessible by any accelerator experiment; it can only be probed by virtual processes such as with proton decay.
- GUTs usually predict the relative branching fractions of different nucleon decay modes. Testing these predictions would, however, require a sizeable sample of proton decay events.
- The dominant proton decay mode of a GUT is often sufficient to roughly identify the likely characteristics of the GUT, such as gauge mediation or the involvement of supersymmetry.

The observation of even a single unambiguous proton decay event would corroborate the idea of unification and the signature of the decay would give strong guidance as to the nature of the underlying theory.

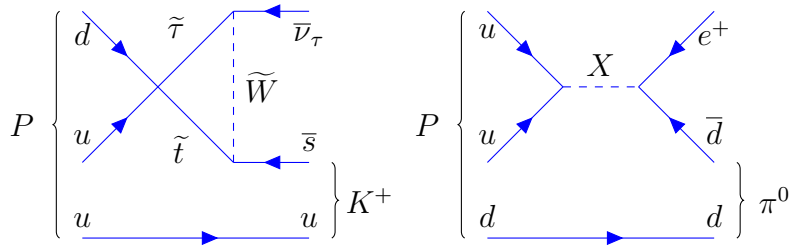

Figure 2.10: Feynman diagrams for proton decay modes from supersymmetric GUT, $p^+ \to K^+\overline{\nu}$ (left) and gauge-mediation GUT models, $p^+ \to e^+\pi^0$ (right).

2.3.2 Proton Decay Modes

From the body of literature, two decay modes (shown in Figure 2.10) emerge that dominate the LBNE experimental design. The more well-known of the two, the decay mode of $p \to e^+\pi^0$, arises from gauge mediation. It is often predicted to have the higher branching fraction and is also demonstrably the more straightforward experimental signature for a water Cherenkov detector. In this mode, the total mass of the proton is converted into the electromagnetic shower energy of the positron and two photons from π^0 decay, with a net momentum vector near zero.

The second key mode is $p \to K^+\overline{\nu}$. This mode is dominant in most supersymmetric GUTs, many of which also favor additional modes involving kaons in the final state. This decay mode with a charged kaon is uniquely interesting; since stopping kaons have a higher ionization density than other particles, a LArTPC could detect it with extremely high efficiency, as described in Chapter 5. In addition, many final states of K^+ decay would be fully reconstructable in a LArTPC.

There are many other allowed modes of proton or bound neutron into antilepton plus meson decay that conserve $B - L$[§], but none of these will influence the design of a next-generation experiment. The most stringent limits, besides those on $p \to e^+\pi^0$, include the lifetime limits on $p \to \mu^+\pi^0$ and $p \to e^+\eta$, both of which are greater than 4×10^{33} years [63]. Any experiment that will do well for $p \to e^+\pi^0$ will also do well for these decay modes. The decays $p \to \overline{\nu}\pi^+$ or $n \to \overline{\nu}\pi^0$ may have large theoretically predicted branching fractions, but they are experimentally difficult due to the sizeable backgrounds from atmospheric-neutrino interactions. The decay $p \to \mu^+K^0$ can be detected relatively efficiently by either water Cherenkov or LArTPC detectors.

A number of other possible modes exist, such as those that conserve $B+L$, that violate only baryon number, or that decay into only leptons. These possibilities are less well-motivated theoretically, as they do not appear in a wide range of models, and are therefore not considered here.

Figure 2.11 shows a comparison of experimental limits, dominated by recent results from Super–Kamiokande to the ranges of lifetimes predicted by an assortment of GUTs. At this time, the theory

[§]In these models, the quantum number $B - L$ is expected to be conserved even though B and L are not individually conserved.

literature does not attempt to precisely predict lifetimes, concentrating instead on suggesting the dominant decay modes and relative branching ratios. The uncertainty in the lifetime predictions comes from details of the theory, such as masses and coupling constants of unknown heavy particles, as well as poorly known details of matrix elements for quarks within the nucleon.

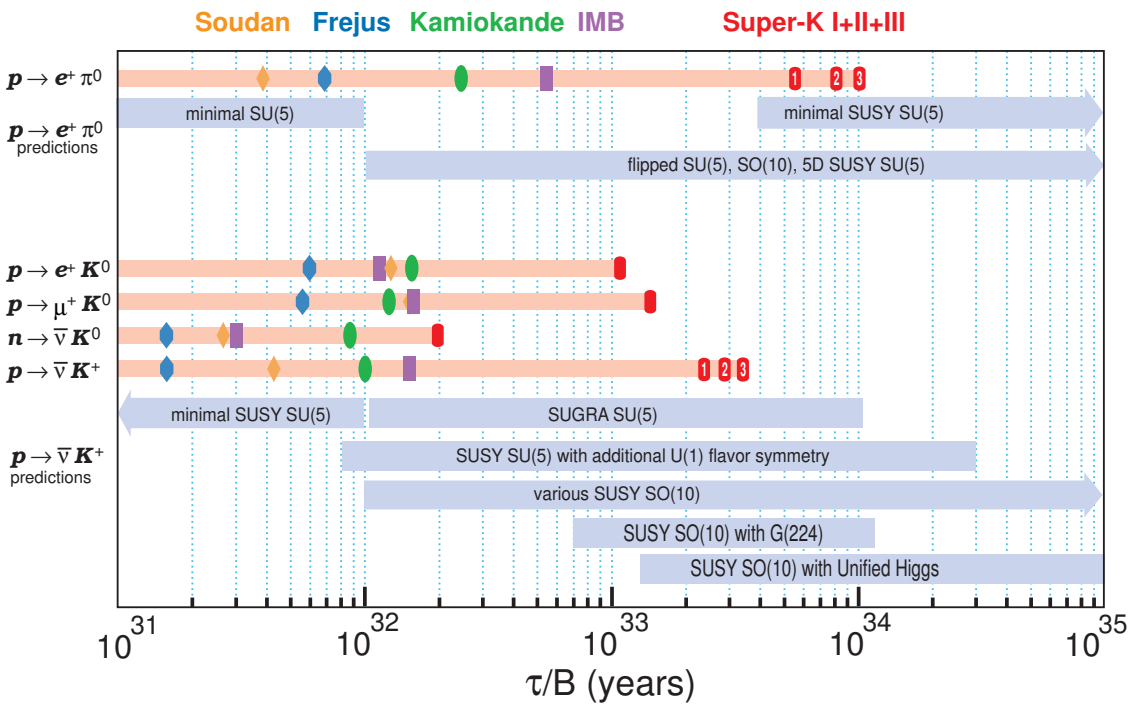

Figure 2.11: Proton decay lifetime limits [16,63] compared to lifetime ranges predicted by Grand Unified Theories. The upper section is for $p \to e^+\pi^0$, most commonly caused by gauge mediation. The lower section is for SUSY-motivated models, which commonly predict decay modes with kaons in the final state. The marker symbols indicate published experimental limits, as indicated by the sequence and colors on top of the figure.

It is apparent from Figure 2.11 that a continued search for proton decay is by no means assured of obtaining a positive result. With that caveat, an experiment with sensitivity to proton lifetimes between 10^{33} and 10^{35} years is searching in the right territory over virtually all GUTs; even if no proton decay is detected, stringent lifetime limits will provide strong constraints on such models. Minimal SU(5) was ruled out by the early work of IMB and Kamiokande and minimal SUSY SU(5) is considered to be ruled out by Super–Kamiokande. In most cases, another order of magnitude in improved limits will not rule out specific models but will constrain their allowed parameters; this could allow identification of models which must be fine-tuned in order to accommodate the data, and are thus less favored.

As Chapter 5 will show, the performance and scalability of the LArTPC technology opens up nucleon decay channels that are not as readily accessible in existing and proposed water Cherenkov detectors, providing LBNE with a unique and compelling opportunity for discovery.

2.4 Supernova-Neutrino Physics and Astrophysics

For over half a century, researchers have been grappling to understand the physics of the neutrino-driven core-collapse supernova. The interest in observing the core-collapse supernova explosion mechanism comes from the key role supernovae of this type have played in the history of the Universe. Without taking supernova feedback into account, for example, modern simulations of galaxy formation cannot reproduce the structure of our galactic disk. More poetically, the heavy elements that are the basis of life on Earth were synthesized inside stars and ejected by supernova explosions.

Neutrinos from a core-collapse supernova are emitted in a burst of a few tens of seconds duration, with about half emitted in the first second. They record the information about the physical processes in the center of the explosion during the first several seconds — as it is happening. Energies are in the few-tens-of-MeV range and luminosity is divided roughly equally between flavors. The basic model of core collapse was confirmed by the observation of neutrino events from SN1987A, a supernova in the Large Magellanic Cloud — outside the Milky Way — 50 kpc (kiloparsecs) away. Nineteen events were detected in two water Cherenkov detectors [64,65] and additional events were reported in a scintillator detector [66]. The neutrino signal from a core-collapse supernova in the Milky Way is expected to generate a high-statistics signal from which LBNE could extract a wealth of information [67,68].

The expected rate of core-collapse supernovae is two to three per century in the Milky Way [69,70]. In a 20-year experimental run, LBNE's probability of observing neutrinos from a core-collapse supernova in the Milky Way is about 40%. The detection of thousands of supernova-burst neutrinos from this event would dramatically expand the science reach of the experiment, allowing observation of the development of the explosion in the star's core and probing the equation-of-state of matter at nuclear densities. In addition, independent measurements of the neutrino mass hierarchy and the θ_{13} mixing angle are possible, as well as additional constraints on physics beyond the Standard Model.

Each of the topics that can be addressed by studying supernova-burst neutrinos represent important outstanding problems in modern physics, each worthy of a separate, dedicated experiment, and the neutrino physics and astrophysics communities would receive payback simultaneously. The opportunity of targeting these topics in a single experiment is very attractive, especially since it may come only at incremental cost to the LBNE Project.

The explosion mechanism is thought to have three distinct stages: the collapse of the iron core, with the formation of the shock and its breakout through the neutrinosphere; the accretion phase, in which the shock temporarily stalls at a radius of about 200 km while the material keeps raining

in; and the cooling stage, in which the hot proto-neutron star loses its energy and trapped lepton number, while the re-energized shock expands to push out the rest of the star. Each of these three stages is predicted to have a distinct signature in the neutrino signal. Thus, it should be possible to directly observe, for example, how long the shock is stalled. More exotic features of the collapse may be observable in the neutrino flux as well, such as possible transitions to quark matter or to a black hole. (An observation in conjunction with a gravitational wave detection would be especially interesting; e.g. [71,72].)

Over the last two decades, neutrino flavor oscillations have been firmly established in solar neutrinos and a variety of terrestrial sources. The physics of the oscillations in the supernova environment promises to be much richer than in any of the cases measured to date, for a variety of reasons:

- Neutrinos travel through the changing profile of the explosion with stochastic density fluctuations behind the expanding shock and, due to their coherent scattering off of each other, their flavor states are coupled.
- The oscillation patterns come out very differently for the normal and inverted mass hierarchies.
- The expanding shock and turbulence leave a unique imprint in the neutrino signal.
- Additional information on oscillation parameters, free of supernova model-dependence, will be available if matter effects due to the Earth can be observed in detectors at different locations around the world [73,74].
- The observation of this potentially copious source of neutrinos will also allow limits on coupling to axions, large extra dimensions, and other exotic physics (e.g., [75,76]).
- The oscillations of neutrinos and antineutrinos from a core-collapse supernova manifest very differently. In the neutrino channel, the oscillation features are in general more pronounced, since the initial spectra of ν_e and ν_μ (ν_τ) are always significantly different. It would be extremely valuable to detect both neutrino and antineutrino channels with high statistics.

Only about two dozen neutrinos were observed from SN1987A, which occurred in a nearby galaxy; in contrast, the currently proposed next-generation detectors would register thousands or tens of thousands of interactions from a core-collapse supernova in our galaxy. The type of observed interactions will depend on the detector technology: a water-Cherenkov detector is primarily sensitive to $\overline{\nu}_e$'s, whereas a LArTPC detector has excellent sensitivity to ν_e's. In each case, the high event rate implies that it should be possible to measure not only the time-integrated spectra, but also their second-by-second evolution. This is a key feature of the supernova-burst physics potential of the planned LBNE experiment.

Currently, experiments worldwide are sensitive primarily to $\overline{\nu}_e$'s, via inverse-beta decay on free protons, which dominates the interaction rate in water and liquid-scintillator detectors. Liquid argon exhibits a unique sensitivity to the ν_e component of the flux, via the absorption interaction on ^{40}Ar, $\nu_e + {}^{40}\mathrm{Ar} \rightarrow e^- + {}^{40}\mathrm{K}^*$. In principle, this interaction can be tagged via the coincidence of the electron and the $^{40}\mathrm{K}^*$ de-excitation gamma cascade. About 900 events would be expected in a 10-kt fiducial liquid argon detector for a core-collapse supernova at 10 kpc. The number of signal events scales with mass and the inverse square of distance, as shown in Figure 2.12. For a collapse

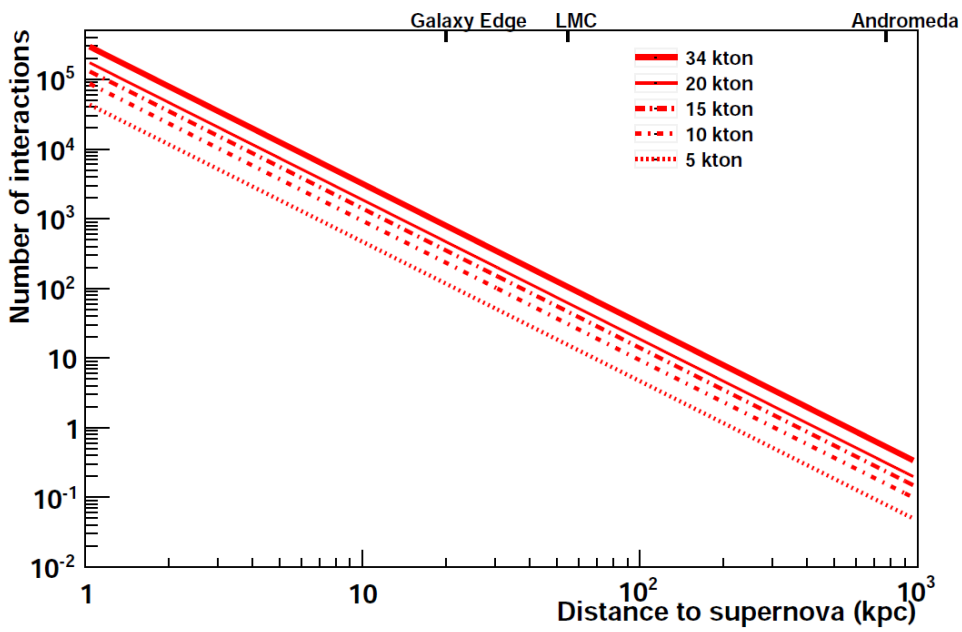

Figure 2.12: Number of supernova neutrino interactions in a liquid argon detector as a function of distance to the supernova for different detector masses. Core collapses are expected to occur a few times per century, at a most-likely distance from 10 kpc to 15 kpc.

in the Andromeda galaxy, massive detectors of hundreds of kilotons would be required to observe a handful of events. However, for supernovae within the Milky Way, even a relatively small 10-kt detector would gather a significant ν_e signal.

Because the neutrinos emerge promptly after core collapse, in contrast to the electromagnetic radiation which must beat its way out of the stellar envelope, an observation could provide a prompt supernova alert [77,78], allowing astronomers to find the supernova in early light turn-on stages, which could yield information about the progenitor (in turn, important for understanding oscillations). Further, observations and measurements by multiple, geographically separated detectors during a core collapse — of which several are expected to be online over the next few decades [67,79] — will enhance the potential science yield from such a rare and spectacular event [73].

References

1. J. Strait, "Physics Research Goals After Reconfiguration," LBNE-doc-3056, 2011.
2. R. Mohapatra, S. Antusch, K. Babu, G. Barenboim, M.-C. Chen, *et al.*, "Theory of neutrinos: A White paper," *Rept.Prog.Phys.* **70** (2007) 1757–1867, arXiv:hep-ph/0510213 [hep-ph].
3. G. Aad *et al.*, **ATLAS Collaboration** , "Observation of a new particle in the search for the Standard Model Higgs boson with the ATLAS detector at the LHC," *Phys.Lett.* **B716** (2012) 1–29, arXiv:1207.7214 [hep-ex].
4. S. Chatrchyan *et al.*, **CMS Collaboration** , "Observation of a new boson at a mass of 125 GeV with the CMS experiment at the LHC," *Phys.Lett.* **B716** (2012) 30–61, arXiv:1207.7235 [hep-ex].
5. DNP/DPF/DAP/DPB Joint Study on the Future of Neutrino Physics, "The Neutrino Matrix.". November, 2004. http://www.aps.org/policy/reports/multidivisional/neutrino/upload/main.pdf.
6. F. An *et al.*, **Daya Bay Collaboration** , "Improved Measurement of Electron Antineutrino Disappearance at Daya Bay," *Chin. Phys.* **C37** (2013) 011001, arXiv:1210.6327 [hep-ex].
7. A. Aguilar-Arevalo *et al.*, **LSND Collaboration** , "Evidence for neutrino oscillations from the observation of anti-neutrino(electron) appearance in a anti-neutrino(muon) beam," *Phys.Rev.* **D64** (2001) 112007, arXiv:hep-ex/0104049 [hep-ex].
8. A. Aguilar-Arevalo *et al.*, **MiniBooNE Collaboration** , "A Search for electron neutrino appearance at the $\Delta m^2 \sim 1\text{eV}^2$ scale," *Phys.Rev.Lett.* **98** (2007) 231801, arXiv:0704.1500 [hep-ex].
9. A. Aguilar-Arevalo *et al.*, **MiniBooNE Collaboration** , "Improved Search for $\overline{\nu_\mu} \to \overline{\nu_e}$ Oscillations in the MiniBooNE Experiment," *Phys.Rev.Lett.* **110** no. 16, (2013) 161801, arXiv:1207.4809 [hep-ex].
10. G. Mention, M. Fechner, T. Lasserre, T. Mueller, D. Lhuillier, *et al.*, "The Reactor Antineutrino Anomaly," *Phys.Rev.* **D83** (2011) 073006, arXiv:1101.2755 [hep-ex].
11. S. F. King, A. Merle, S. Morisi, Y. Shimizu, and M. Tanimoto, "Neutrino Mass and Mixing: from Theory to Experiment," arXiv:1402.4271 [hep-ph], 2014.
12. A. de Gouvea *et al.*, **Intensity Frontier Neutrino Working Group** , "Neutrinos," FERMILAB-CONF-13-479-E, arXiv:1310.4340 [hep-ex], 2013.
13. P. Harrison, D. Perkins, and W. Scott, "Tri-bimaximal mixing and the neutrino oscillation data," *Phys.Lett.* **B530** (2002) 167, arXiv:hep-ph/0202074 [hep-ph].
14. C. H. Albright and M.-C. Chen, "Model Predictions for Neutrino Oscillation Parameters," *Phys.Rev.* **D74** (2006) 113006, arXiv:hep-ph/0608137 [hep-ph].

15. G. Fogli, E. Lisi, A. Marrone, D. Montanino, A. Palazzo, *et al.*, "Global analysis of neutrino masses, mixings and phases: entering the era of leptonic CP violation searches," *Phys.Rev.* **D86** (2012) 013012, `arXiv:1205.5254 [hep-ph]`.
16. J. Beringer *et al.*, **Particle Data Group** , "Review of Particle Physics (RPP)," *Phys.Rev.* **D86** (2012) 010001.
17. C. Jarlskog, "A Basis Independent Formulation of the Connection Between Quark Mass Matrices, CP Violation and Experiment," *Z.Phys.* **C29** (1985) 491–497.
18. A. Meroni, S. Petcov, and M. Spinrath, "A SUSY SU(5)xT' Unified Model of Flavour with large θ_{13}," *Phys.Rev.* **D86** (2012) 113003, `arXiv:1205.5241 [hep-ph]`.
19. G.-J. Ding, S. F. King, and A. J. Stuart, "Generalised CP and A_4 Family Symmetry," *JHEP* **1312** (2013) 006, `arXiv:1307.4212`.
20. C. Luhn, "Trimaximal TM_1 neutrino mixing in S_4 with spontaneous CP violation," *Nucl.Phys.* **B875** (2013) 80–100, `arXiv:1306.2358 [hep-ph]`.
21. G.-J. Ding and Y.-L. Zhou, "Predicting Lepton Flavor Mixing from $\Delta(48)$ and Generalized CP Symmetries," `arXiv:1312.5222 [hep-ph]`, 2013.
22. S. Antusch, S. F. King, and M. Spinrath, "Spontaneous CP violation in $A_4 \times SU(5)$ with Constrained Sequential Dominance 2," *Phys.Rev.* **D87** no. 9, (2013) 096018, `arXiv:1301.6764 [hep-ph]`.
23. S. F. King, "A model of quark and lepton mixing," *JHEP* **1401** (2014) 119, `arXiv:1311.3295 [hep-ph]`.
24. E. Kolb and M. Turner, *The Early Universe*. Westview Press, 1994. ISBN 978-0201626742.
25. S. Weinberg, *Cosmology*. Oxford University Press, USA, first ed., April, 2008. ISBN 978-0198526827.
26. G. Steigman, "Primordial Nucleosynthesis in the Precision Cosmology Era," *Ann.Rev.Nucl.Part.Sci.* **57** (2007) 463–491, `arXiv:0712.1100 [astro-ph]`.
27. M. Fukugita and T. Yanagida, "Baryogenesis Without Grand Unification," *Phys.Lett.* **B174** (1986) 45.
28. T. Yanagida, "Horizontal Symmetry and Masses of Neutrinos," *Prog.Theor.Phys.* **64** (1980) 1103.
29. S. Pascoli, S. Petcov, and A. Riotto, "Leptogenesis and Low Energy CP Violation in Neutrino Physics," *Nucl.Phys.* **B774** (2007) 1–52, `arXiv:hep-ph/0611338 [hep-ph]`.
30. F. Capozzi, G. Fogli, E. Lisi, A. Marrone, D. Montanino, *et al.*, "Status of three-neutrino oscillation parameters, circa 2013," `arXiv:1312.2878 [hep-ph]`, 2013.
31. P. Adamson *et al.*, **MINOS Collaboration** , "Search for the disappearance of muon antineutrinos in the NuMI neutrino beam," *Phys.Rev.* **D84** (2011) 071103, `arXiv:1108.1509 [hep-ex]`.
32. S. Mikheev and A. Y. Smirnov, "Resonance Amplification of Oscillations in Matter and Spectroscopy of Solar Neutrinos," *Sov.J.Nucl.Phys.* **42** (1985) 913–917.
33. L. Wolfenstein, "Neutrino Oscillations in Matter," *Phys.Rev.* **D17** (1978) 2369–2374.

34. G. Bellini *et al.*, **Borexino Collaboration** , "Measurement of the solar 8B neutrino rate with a liquid scintillator target and 3 MeV energy threshold in the Borexino detector," *Phys.Rev.* **D82** (2010) 033006, `arXiv:0808.2868 [astro-ph]`.
35. G. Bellini, J. Benziger, D. Bick, S. Bonetti, G. Bonfini, *et al.*, "Precision measurement of the 7Be solar neutrino interaction rate in Borexino," *Phys.Rev.Lett.* **107** (2011) 141302, `arXiv:1104.1816 [hep-ex]`.
36. B. Aharmim *et al.*, **SNO Collaboration** , "Combined Analysis of all Three Phases of Solar Neutrino Data from the Sudbury Neutrino Observatory," *Phys.Rev.* **C88** (2013) 025501, `arXiv:1109.0763 [nucl-ex]`.
37. A. Renshaw *et al.*, **Super-Kamiokande Collaboration** , "First Indication of Terrestrial Matter Effects on Solar Neutrino Oscillation," `arXiv:1312.5176 [hep-ex]`, 2013.
38. M. Freund, "Analytic approximations for three neutrino oscillation parameters and probabilities in matter," *Phys.Rev.* **D64** (2001) 053003, `arXiv:hep-ph/0103300 [hep-ph]`.
39. W. Marciano and Z. Parsa, "Intense neutrino beams and leptonic CP violation," *Nucl.Phys.Proc.Suppl.* **221** (2011) 166–172, `arXiv:hep-ph/0610258 [hep-ph]`.
40. B. Viren, "libnuosc++ - A library for calculating 3 neutrino oscillation probabilities.." `https://github.com/brettviren/nuosc`.
41. A. M. Dziewonski and D. L. Anderson, "Preliminary reference Earth model," *Phys. Earth Plan. Int.* **25** (1981) 297.
42. J. Appel *et al.*, "Physics Working Group Report to the LBNE Reconfiguration Steering Committee," 2012. `http://www.fnal.gov/directorate/lbne_reconfiguration/files/LBNE-Reconfiguration-PhysicsWG-Report-August2012.pdf`.
43. R. Brun, F. Bruyant, M. Maire, A. McPherson, and P. Zanarini, "GEANT3," CERN-DD-EE-84-1, 1987.
44. M. Bass *et al.*, **LBNE Collaboration** , "Baseline optimization for the measurement of CP violation and mass hierarchy in a long-baseline neutrino oscillation experiment," FERMILAB-PUB-13-506-E, `arXiv:1311.0212 [hep-ex]`, 2013.
45. M. Raidal, "Relation between the neutrino and quark mixing angles and grand unification," *Phys.Rev.Lett.* **93** (2004) 161801, `arXiv:hep-ph/0404046 [hep-ph]`.
46. H. Minakata and A. Y. Smirnov, "Neutrino mixing and quark-lepton complementarity," *Phys.Rev.* **D70** (2004) 073009, `arXiv:hep-ph/0405088 [hep-ph]`.
47. A. Y. Smirnov, "Neutrino mass, mixing and discrete symmetries," *J.Phys.Conf.Ser.* **447** (2013) 012004, `arXiv:1305.4827 [hep-ph]`.
48. J. Harada, "Non-maximal θ_{23}, large θ_{13} and tri-bimaximal θ_{12} via quark-lepton complementarity at next-to-leading order," *Europhys.Lett.* **103** (2013) 21001, `arXiv:1304.4526 [hep-ph]`.
49. B. Hu, "Trimaximal-Cabibbo neutrino mixing: A parametrization in terms of deviations from tribimaximal mixing," *Phys.Rev.* **D87** no. 5, (2013) 053011, `arXiv:1212.4079 [hep-ph]`.

50. P. Ramond, "Fundamental Physics Underground. Presentation at ISOUPS (International Symposium: Opportunities in Underground Physics for Snowmass), Asilomar, May 2013," 2013.
51. S. Antusch, C. Biggio, E. Fernandez-Martinez, M. Gavela, and J. Lopez-Pavon, "Unitarity of the Leptonic Mixing Matrix," *JHEP* **0610** (2006) 084, `arXiv:hep-ph/0607020 [hep-ph]`.
52. X. Qian, C. Zhang, M. Diwan, and P. Vogel, "Unitarity Tests of the Neutrino Mixing Matrix," `arXiv:1308.5700 [hep-ex]`, 2013.
53. J. C. Pati and A. Salam, "Is Baryon Number Conserved?," *Phys.Rev.Lett.* **31** (1973) 661–664.
54. H. Georgi and S. Glashow, "Unity of All Elementary Particle Forces," *Phys.Rev.Lett.* **32** (1974) 438–441.
55. S. Dimopoulos, S. Raby, and F. Wilczek, "Proton Decay in Supersymmetric Models," *Phys.Lett.* **B112** (1982) 133.
56. P. Langacker, "Grand Unified Theories and Proton Decay," *Phys.Rept.* **72** (1981) 185.
57. W. de Boer, "Grand unified theories and supersymmetry in particle physics and cosmology," *Prog.Part.Nucl.Phys.* **33** (1994) 201–302, `arXiv:hep-ph/9402266 [hep-ph]`.
58. P. Nath and P. Fileviez Perez, "Proton stability in grand unified theories, in strings and in branes," *Phys.Rept.* **441** (2007) 191–317, `arXiv:hep-ph/0601023 [hep-ph]`.
59. S. Raby, T. Walker, K. Babu, H. Baer, A. Balantekin, *et al.*, "DUSEL Theory White Paper," SLAC-PUB-14734, FERMILAB-PUB-08-680-T, `arXiv:0810.4551 [hep-ph]`, 2008.
60. G. Senjanovic, "Proton decay and grand unification," *AIP Conf.Proc.* **1200** (2010) 131–141, `arXiv:0912.5375 [hep-ph]`.
61. T. Li, D. V. Nanopoulos, and J. W. Walker, "Elements of F-ast Proton Decay," *Nucl.Phys.* **B846** (2011) 43–99, `arXiv:1003.2570 [hep-ph]`.
62. E. Noether, "Invariant Variation Problems," *Gott.Nachr.* **1918** (1918) 235–257, `arXiv:physics/0503066 [physics]`.
63. H. Nishino *et al.*, **Super-Kamiokande Collaboration** , "Search for Nucleon Decay into Charged Anti-lepton plus Meson in Super-Kamiokande I and II," *Phys.Rev.* **D85** (2012) 112001, `arXiv:1203.4030 [hep-ex]`.
64. R. Bionta, G. Blewitt, C. Bratton, D. Casper, A. Ciocio, *et al.*, "Observation of a Neutrino Burst in Coincidence with Supernova SN 1987a in the Large Magellanic Cloud," *Phys.Rev.Lett.* **58** (1987) 1494.
65. K. Hirata *et al.*, **KAMIOKANDE-II Collaboration** , "Observation of a Neutrino Burst from the Supernova SN 1987a," *Phys.Rev.Lett.* **58** (1987) 1490–1493.
66. E. Alekseev, L. Alekseeva, V. Volchenko, and I. Krivosheina, "Possible Detection of a Neutrino Signal on 23 February 1987 at the Baksan Underground Scintillation Telescope of the Institute of Nuclear Research," *JETP Lett.* **45** (1987) 589–592.
67. K. Scholberg, "Supernova neutrino detection," *Nucl.Phys.Proc.Suppl.* **221** (2011) 248–253, `arXiv:astro-ph/0701081 [astro-ph]`.

68. A. Dighe, "Physics potential of future supernova neutrino observations," *J.Phys.Conf.Ser.* **136** (2008) 022041, arXiv:0809.2977 [hep-ph].
69. G. A. Tammann, W. Loeffler, and A. Schroder, "The Galactic supernova rate," *Astrophys. J. Suppl.* **92** (1994) 487–493.
70. E. Cappellaro, R. Evans, and M. Turatto, "A new determination of supernova rates and a comparison with indicators for galactic star formation," *Astron.Astrophys.* **351** (1999) 459, arXiv:astro-ph/9904225 [astro-ph].
71. G. Pagliaroli, F. Vissani, E. Coccia, and W. Fulgione, "Neutrinos from Supernovae as a Trigger for Gravitational Wave Search," *Phys. Rev. Lett.* **103** (2009) 031102, arXiv:0903.1191 [hep-ph].
72. C. Ott, E. O'Connor, S. Gossan, E. Abdikamalov, U. Gamma, *et al.*, "Core-Collapse Supernovae, Neutrinos, and Gravitational Waves," *Nucl.Phys.Proc.Suppl.* **235-236** (2013) 381–387, arXiv:1212.4250 [astro-ph.HE].
73. A. Mirizzi, G. Raffelt, and P. Serpico, "Earth matter effects in supernova neutrinos: Optimal detector locations," *JCAP* **0605** (2006) 012, arXiv:astro-ph/0604300 [astro-ph].
74. S. Choubey, B. Dasgupta, A. Dighe, and A. Mirizzi, "Signatures of collective and matter effects on supernova neutrinos at large detectors," arXiv:1008.0308 [hep-ph], 2010.
75. G. G. Raffelt, "Astrophysical axion bounds: An Update," arXiv:astro-ph/9707268 [astro-ph], 1997.
76. S. Hannestad and G. Raffelt, "New supernova limit on large extra dimensions," *Phys.Rev.Lett.* **87** (2001) 051301, arXiv:hep-ph/0103201 [hep-ph].
77. P. Antonioli *et al.*, "Snews: The supernova early warning system," *New J. Phys.* **6** (2004) 114, astro-ph/0406214.
78. K. Scholberg, "The SuperNova Early Warning System," *Astron. Nachr.* **329** (2008) 337–339, arXiv:0803.0531 [astro-ph].
79. K. Scholberg, "Future supernova neutrino detectors," *J.Phys.Conf.Ser.* **203** (2010) 012079.